New directions in the development of drift chambers

B. Sitar

Joint Institute for Nuclear Research, Dubna

Fiz. Elem. Chastits At. Yadra **18**, 1080–1124 (September–October 1987)

New directions in the development of drift chambers are considered. The main factors that determine their coordinate accuracy are discussed. New methods of improving their spatial resolution are analyzed. The characteristics of the large multilayer (time projection) chambers used in recent years in high-energy collider and extracted-beam experiments are described. The factors that influence the counting rates of such chambers, the methods of their calibration, and operation in a magnetic field are analyzed. Wide-gap and also electrodeless chambers and the possibilities of using them in modern physics experiments are described.

INTRODUCTION

Drift chambers have already been used for more than 15 years in physics experiments.

The determination of particle coordinates through measurement of electron drift time was first proposed by the group of Charpak.[1,2] The first drift chambers were constructed by Walenta *et al.*[3] and Saudinos *et al.*[4] at the beginning of the seventies. Since then, they have become one of the basic forms of coordinate detectors employed in large high-energy facilities. Drift chambers are distinguished by a high spatial resolution, a relatively small number of electronics channels, and uncomplicated construction.

The basic principles of drift chambers have been considered in monographs and review papers (see, for example, Refs. 5–9).

Although the characteristics of drift chambers have been well studied, several new ideas for their improvement have recently been advanced. Some new directions in the development of drift chambers can now be discerned.

1. High-precision drift chambers. In these, different means are employed in the attempt to achieve a limiting spatial resolution of about 30 μm and a two-track resolution of 100–200 μm.

2. Multilayer chambers. These are large coordinate detectors with a space divided into many layers, in which the coordinates of the tracks in space are repeatedly measured. In addition, in such chambers charged particles are identified by multiple measurement of the ionization energy losses.[9] Multilayer chambers are used as the central detectors of charged particles in practically all large collider facilities.

3. Wide-gap drift chambers. They are often called "economic" drift chambers. They are distinguished by their large electron drift length and small number of electronics channels. They are used in large high-energy facilities above all in conjunction with electromagnetic or hadronic calorimeters and muon detectors; they can have applications in large neutrino detectors and underground detectors looking for decay of nucleons or new phenomena in cosmic-ray physics.

4. Chambers with longitudinal electron drift. In such chambers, the electrons drift along the particle trajectory. They are used to identify charged particles by counting the number of primary ionization clusters. Such chambers are described, for example, in Ref. 9.

5. Drift chambers in self-quenching streamer regime.[10] The use of the self-quenching streamer regime instead of the proportional regime in a drift chamber leads to a simplification of the electronics channels. These questions are discussed in Ref. 11.

In this review, we describe new directions in the development of drift chambers aimed at their further improvement.

1. SPATIAL RESOLUTION OF DRIFT CHAMBERS

Main factors that determine the coordinate accuracy of drift chambers

The track coordinate x in the direction normal to the plane of the anode wires is determined in a drift chamber by measuring the time interval between the instant t_0 at which the particle passes through the chamber and the time t_1 of arrival of the swarm of electrons from the track of the particle at the anode:

$$x = \int_{t_0}^{t_1} w_d \, dt; \tag{1}$$

if the drift velocity w_d is constant, then

$$x = w_d t_d, \tag{2}$$

where the electron drift time is $t_d = t_1 - t_0$.

A constant drift velocity in a certain interval of electric field strengths can be ensured by an appropriate choice of the gas mixture. In a number of gas mixtures, one can ensure a constant drift velocity in a wide range of field strengths (Fig. 1). The dependences of the drift velocity on the field strength for a large number of mixtures can be found in Ref. 12. Another condition for accurate operation of the drift chamber is homogeneity of the electric field in the drift space $[E(x) \approx \text{const}]$.

Basic types of construction of proportional and drift chambers

Figure 2a shows the scheme of a proportional chamber. The scheme without field-shaping electrodes (Fig. 2b) is usually employed in narrow-gap drift chambers designed for accurate determination of trajectory coordinates in high particle fluxes. Drift chambers with field-shaping wires to which a linearly decreasing potential is applied (Fig. 2c) are characterized by a high homogeneity of the electric field. Such a geometry of the wires is used in the majority of planar drift chambers used as coordinate detectors. A configuration of electrodes of the type shown in Fig. 2d is used in some cylindrical drift chambers. The arrangement of the electrodes shown in Fig. 2e is typical of multilayer drift cham-

 0090-4759/87/050460-20$04.40

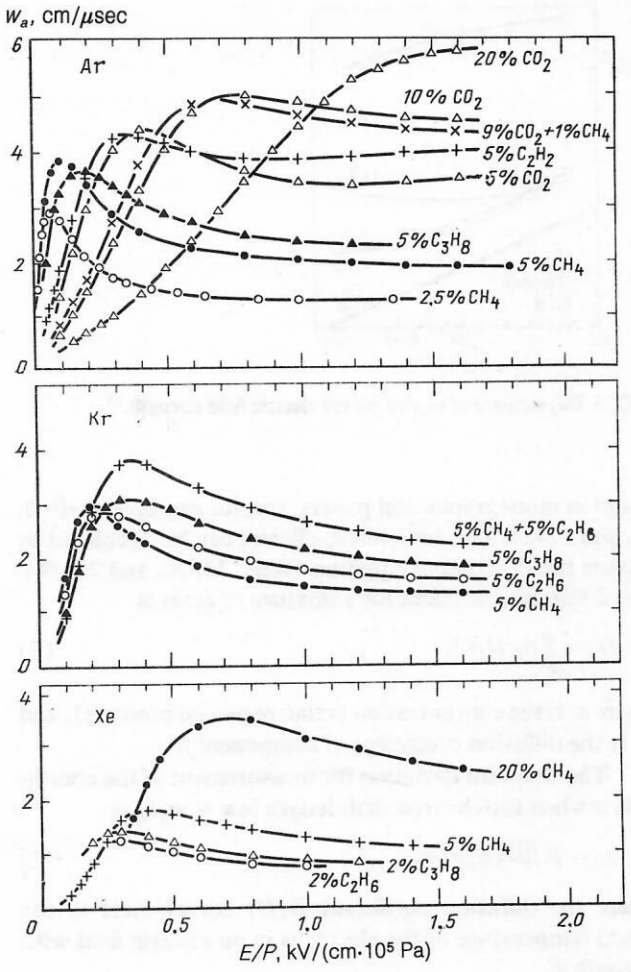

FIG. 1. Electron drift velocity w_d in mixtures of Ar, Kr, Xe with hydrocarbons and CO_2.[90]

bers (for example, the cylindrical chambers of JET type).[9]

To ensure a higher field homogeneity, the drift space in time-projection chambers[9] is separated from the region of the signal wires by a plane of additional wires (Fig. 2f).

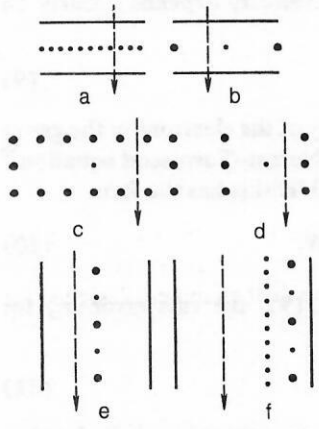

FIG. 2. Arrangement of wires in different types of chamber; a) proportional chamber; b) planar drift chamber; c) drift chamber with field-shaping electrodes; d) element of a cylindrical drift chamber; e) drift chamber of JET type; f) drift chamber of time-projection type; the larger black circles represent the field-shaping electrodes, the small black circles the signal wires, the continuous lines the cathode, and the broken lines the particle trajectory.

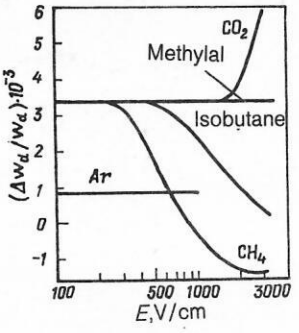

FIG. 3. Relative change $\Delta w_d/w_d$ in the drift velocity for an increase of the temperature by 1 °C under normal conditions as a function of E.[13]

Constancy of the electron drift velocity

Constancy of the electron drift velocity is a necessary condition for exact measurement of coordinates in a drift chamber—the drift time must depend linearly on the track coordinate [see (2)]. In the majority of drift chambers, this condition can be realized to a high accuracy over the complete volume except for regions near the signal wire and at the edge of the chamber, where a strong gradient of the electric field is observed. The condition (2) is valid for tracks of particles perpendicular to the direction of electron drift.

In the case of prolonged operation of a drift chamber, it is necessary to maintain constancy of the drift velocity, and for this it is necessary to stabilize the electric field strength, the composition of the gas, its pressure, and the temperature. The relative change $\Delta w_d/w_d$ in the drift velocity corresponding to a change in the temperature by 1 °C is shown as a function of the electric field strength in Fig. 3. For a number of organic gases, the ratio $\Delta w_d/w_d = 3.4\cdot 10^{-3}$/°C does not depend on E at low field strengths.[13]

Rms error in the measurement of the coordinate of a particle trajectory in a drift chamber

The rms error σ_x is determined by the expression

$$\sigma_x^2 = \sigma_s^2 + \sigma_{D'}^2 + \sigma_A^2, \qquad (3)$$

which takes into account the errors due to the distribution of the primary ionization clusters[9] along the particle trajectory (σ_s), the diffusion of the electron swarm in the electric field ($\sigma_{D'}$), and the instrumental errors (σ_A), which include the instrumental resolution, the fluctuations of the gas multiplication, etc.

We estimate the values of these errors. Suppose that a particle has passed at a certain distance x from the signal wire and over 1 cm of track length has created in the gas N_c primary ionization clusters (Fig. 4). The first electron (cluster) reaches the wire after the time $t_1 = x_1/w_d$, where x_1 is the length of its trajectory. The probability of finding the electron at distance y_1 from the coordinate axis is

$$\mathcal{P}(y_1) = 2N_c e^{-2N_c y_1}, \qquad (4)$$

from which we conclude that the *standard deviation of the distribution of the lengths* x_1 *is*[14]

$$\sigma_s = \sqrt{\frac{5}{16}}\frac{1}{N_c^2 x} \qquad (5)$$

for $x \gg 1/N_c$.

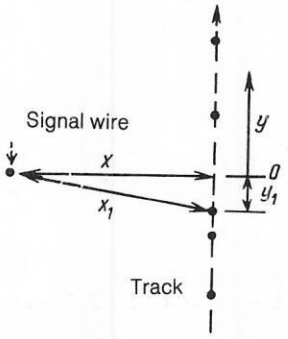

FIG. 4. Distribution of electrons on the particle track in a drift chamber.

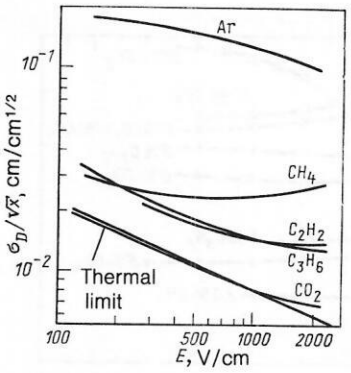

FIG. 6. Dependence of $\sigma_D/\sqrt{x}$ on the electric field strength.[14]

The spread of the electrons around the track after their thermalization, which is characterized by σ_{xt}, also contributes to σ_s. The electron energy supplied by ionization collisions of the particle with atoms of the gas is reduced in the process of thermalization by inelastic collisions of the electrons with the atoms to the mean energy $\varepsilon_e = 3kT/2$ corresponding to the equilibrium thermal motion of electrons in the gas.

The mean displacement length l_t of an electron due to thermalization (the thermalization length) in a proportional detector is not large. For example, in argon under normal conditions and $E = 1$ kV/cm and $\varepsilon_e \approx 4$ eV the length is $l_t \approx 0.5\ \mu$m for an electron from the M shell, about 1 μm from the L shell, and about 15 μm from the K shell.[15] It is known that the trajectories of the particles in the gas contain mainly isolated electrons (about 80%)[16] with range $\lesssim 1\ \mu$m. Electrons with higher energy (δ electrons) arise seldom, and their range is usually $\leqslant 200\ \mu$m, and this has hardly any effect on the measurement of particle coordinates in drift chambers. In argon and an electric field $E \approx 1$ kV/cm the value of σ_{xt} is of the order of several microns; the mean distance between clusters is $\approx 300\ \mu$m, so that $\sigma_{xt} \ll \sigma_s$. The calculated dependence of σ_s on the drift length x is shown in Fig. 5. We recall that in argon $\overline{N}_c \approx 30\ \text{cm}^{-1}$.

In the case of a large electron drift length, the main contribution to the spatial resolution is made by the *diffusion term* $\sigma_{D'}$. The values of $\sigma_{D'}$ measured in drift chambers differ appreciably from the value of σ_D determined by the well-known relation

$$\sigma_D(t_d) = l_D = \sqrt{2Dt_d}, \tag{6}$$

where D is the diffusion coefficient. The quantity l_D is called the electron diffusion displacement. The determination of the diffusion coefficient and its values for many gases can be found in monographs and papers; see, for example, Refs. 9, 10, and 17–21. The diffusion coefficient can be calculated by solving the Boltzmann equation (Refs. 13, 20, and 22–24). The diffusion coefficient for a mixture of gases is

$$D = (\sum_j a_j/D_j)^{-1}, \tag{7}$$

where a_j is the concentration (relative partial pressure), and D_j is the diffusion coefficient of component j.

The standard deviation for measurement of the coordinate x when the electron drift length is $x = w_d t_d$ is

$$\sigma_D = \sqrt{2D(E)\, x/w_d}, \tag{8}$$

where the diffusion coefficient $D(E)$ corresponds to the raised temperature of the electrons in an electric field with strength E.

The dependences $\sigma_D(E)$ for a number of gases are given in Fig. 6. The values of σ_D differ appreciably because of the differences in the energies acquired by the electrons in the electric field. In some so-called cool gases (CO_2, NH_3, isobutane, methylal vapor) the electron energy remains thermal up to relatively high values of the electric field strength. This is due to the large cross section of elastic collisions in such gases. For example, in CO_2 and isobutane a Maxwellian energy distribution of the electrons is maintained up to $E = 200$–300 V/cm, and in NH_3 even up to ≈ 700 V/cm. In such gases, the electron drift velocity depends linearly on E/p:

$$w_d = \mu E/P, \tag{9}$$

where $\mu = \text{const}$ is the mobility of the electrons in the gas at pressure P. In cool gases, the Nernst–Townsend equation[20] holds; for $P = 10^5$ Pa, $T = 300$ °K this has the form

$$\frac{D}{\mu} = \frac{kT}{e} = \frac{2}{3}\bar{\varepsilon}_e \approx 0.026\ \text{eV}. \tag{10}$$

With allowance for (8) and (9), the rms error σ_D for $p = 10^5$ Pa is

$$\sigma_D(E) = \sqrt{2kTx/(eE)}. \tag{11}$$

The accuracy of coordinate measurement in a drift chamber cannot exceed this quantity which is called the *thermal limit* due to diffusion.

The diffusion coefficient is different in the directions along and at right angles to the electric field. In many gases, the longitudinal *diffusion coefficient* (in the direction of the

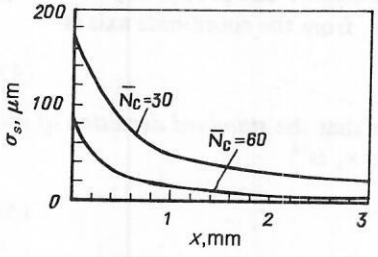

FIG. 5. Dependence of σ_s on the electron drift length x.[14]

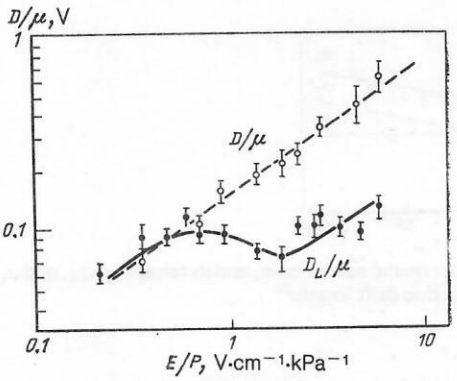

FIG. 7. Coefficients of electron diffusion $D(E)/\mu$ and $D_L(E)/\mu$ as functions of the electric field strength in the drift chamber JADE (Ref. 30) containing 87.2% argon, 10% methane, and 2.8% isobutane at $p = 404$ kPa.

lines of force of the electric field) satisfies $D_L < D$ (see Ref. 12). As an example, Fig. 7 gives the dependences $D/\mu(E)$ and $D_L/\mu(E)$ for a gas mixture often used in drift chambers.

The decrease in the diffusion in the direction parallel to E is explained by the fact that the electrons at the leading edge of the cloud diffuse predominantly in the direction of motion of the electron swarm, and therefore the electric field accelerates them more strongly. Because of this, their mean range l_e is reduced, and this leads to a reduction of their drift velocity[6,13]:

$$w_d \approx \frac{2}{3}\frac{eEl_e}{m_e\bar{v}_e},$$

where m_e is the mass of the electron and $\bar{v}_e$ is its mean velocity.

Conversely, electrons at the far end of the swarm diffuse predominantly in the direction opposite to the motion of the swarm, and the electric field "decelerates" them; therefore, their range l_e increases, and this gives rise to an increase of their drift velocity. These processes lead to a compression of the electron swarm in the direction of its drift and is the reason why $D_L(E) < D(E)$. The relationship between $D_L(E)$ and $D(E)$ depends on the behavior of the function $l_e(\varepsilon_e)$ (or the cross section $\sigma_e(\varepsilon_e)$ of elastic collisions of the electrons with the atoms of the gas). If l_e decreases with increasing electron energy ε_e, then $D_L(E) < D(E)$; for the opposite dependence $l_e(\varepsilon_e)$, it may happen that $D_L(E) > D(E)$. Therefore, the ratio $D_L(E)/D(E)$ depends on the electric field strength (Fig. 7).

The differences between $D_L(E)$ and $D(E)$ were first discovered by Wagner *et al.*[25] Calculations of the coefficient of longitudinal diffusion have been made by Parker and Lowke[26] and Skullerud.[27]

In argon at certain E/P values, the difference between $D_L(E)$ and $D(E)$ is very appreciable: $D(E) \approx 7D_L(E)$.[26] In krypton and xenon the functions $D_L(E)/\mu(E)$ and $D(E)/\mu(E)$ are close to their values for argon. In other gases, the ratio $D(E)/D_L(E)$ is not so large. However, in an estimate of the influence of diffusion on the accuracy of coordinate measurement in a drift chamber it is necessary to take into account the longitudinal component of the diffusion, and therefore (8) takes the form

$$\sigma_D = \sqrt{2D_L(E)\,t_d} = \sqrt{2D_L(E)\,x/w_d}. \qquad (12)$$

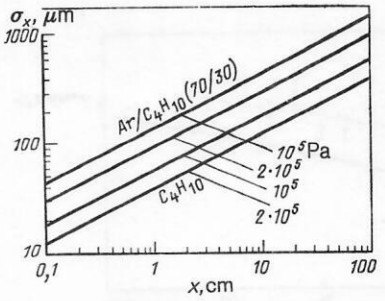

FIG. 8. Calculated dependence of σ_x [with allowance for $D_L(E)$] on the electron drift length.[14]

The results of measurements of the dependence $D_L(E/P)$ for different gases and mixtures of them can be found, for example, in Refs. 12 and 28.

Because of the diffusion, the spatial resolution becomes less good with increasing drift length x in the proportion $\sqrt{x}$ (Fig. 8) but is improved by an increase in the gas pressure.

The difference between σ_D and $\sigma_{D'}$ is due to the fact that electrons from different sections of the track arrive at different times at the signal wire. This happens because the electric field near the wire is not homogeneous but cylindrically symmetric, and therefore the path of electrons from the edge of the layer to the signal wire is longer than the path of electrons from the center of the layer. In Fig 9 the continuous lines show the trajectories of the electrons in the chamber JADE, while the broken lines are the isochrones. It can be seen that electrons from different sections of the particle trajectory arrive at the signal wire at different times. This must be taken into account when one is determining the spatial resolution of a drift chamber.

The spatial resolution also depends on the method used to detect the electron swarm on the signal wire. In the case of triggering of the electronics by the leading edge of the signal and a minimal detection threshold, the spatial resolution corresponding to the arrival of the first electron at the wire is[13]

$$\sigma_1 = \frac{1.28\sigma_D}{\sqrt{2\ln N_c}}. \qquad (13)$$

Another method is based on using the centroid of the collected charge as the time marker. In this case, the rms error in

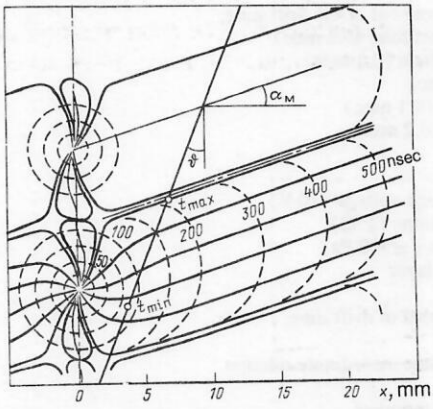

FIG. 9. Electron trajectories in the drift chamber JADE.[30]

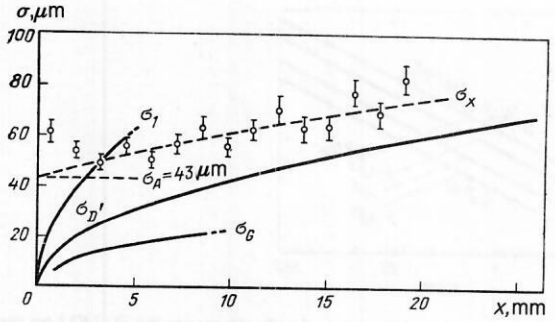

FIG. 10. Dependences of σ_1, σ_G, $\sigma_{D'}$, σ_A, and σ_x on the drift length. The open circles are the experimental data for pions with $p = 150$ GeV/c.[13]

the measurement of the coordinate x is

$$\sigma_G = \sigma_D/\sqrt{N_e}. \tag{14}$$

Figure 10 gives the dependences $\sigma_1(x)$ and $\sigma_G(x)$ for $\sigma_D = \sqrt{2\varepsilon_k x/eE}$. It can be seen that in a real detector the dependence $\sigma_{D'}(x)$ lies between the extreme cases σ_1 and σ_G, since triggering of the electronics usually occurs after the arrival of several electrons at the signal wire. As a result, $\sigma_{D'}$ is 2–3 times less than σ_D.

The instrumental resolution, σ_A, depends in the first place on the accuracy of the construction of the chamber and on the quality of the electronics. For high-precision drift chambers, $\sigma_A = 20$–$50\ \mu$m.

The total effect of all the factors that we have considered determines the rms error σ_x (3) in the measurement of coordinates in a drift chamber. The dependence of σ_x on the drift length is given in Fig. 11, which shows that at distances several millimeters from the wire the accuracy of the coordinate determination is about $50\ \mu$m.[29] The conditions realized in Ref. 14 in the achievement of a resolution $\sigma_x \approx 50$–$55\ \mu$m are listed in Table I.

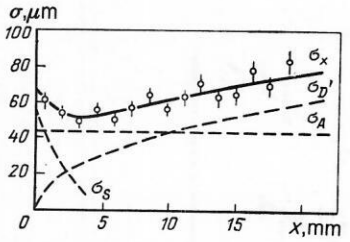

FIG. 11. Drift-chamber spatial resolution σ_x and its terms $\sigma_{D'}$, σ_A, and σ_s as functions of the electron drift length.[29]

The spatial resolution in large drift chambers is 2–3 times less good than the limiting value $\sigma_x \approx 500\ \mu$m. This is due to inaccuracies in the positions of the wires, fluctuations of the pressure and temperature, difficulties in the calibration of large chambers, the dependence of the resolution on the angle of inclination of the track, etc.

An important characteristic of drift chambers is the *two-track resolution*, x_{12}, i.e., the minimal distance between tracks at which they can be separated with a high degree of confidence (80–90%). Typically, $x_{12} \approx 1$ cm. If the electronics detects from each signal wire only one signal, then x_{12} is the distance between the wires. In chambers with electronics capable of processing many signals from one wire, x_{12} is determined in the first place by the signal duration (usually, 150–200 nsec).

2 HIGH-PRECISION DRIFT CHAMBERS

Drift chambers are among the most accurate coordinate detectors, but in a number of physics problems, for example, in the investigation of decays of charmed particles with lifetime $\sim 10^{-13}$ sec, their accuracy must be improved still further. For such problems, it is necessary to have $\sigma_x < 50\ \mu$m and $x_{12} \leqslant 500\ \mu$m. In many laboratories throughout

TABLE I. Contribution of different factors to the spatial resolution $\sigma_x = 50$–$55\ \mu$m achieved in a high-precision drift chamber.[14]

Factors influencing the resolution	Contribution to σ_x, μm
Mechanical inaccuracies:	
positioning of wires	10
gravitational sag of wires (40 μm)	5
electrostatic bias of wire	5
	12
Inaccuracies in measurement of the drift time:	
determination of start time (0.2 nsec)	10
time of flight of particle (0.1 nsec)	5
signal delay (0.1 nsec)	5
calibration of TDC (0.1 nsec)	5
resolution of TDC (0.2 nsec)	10
	17
Chamber parameters:	
fluctuations of the high voltage (10 V)	10
temperature fluctuations (1 °C)	10
pressure fluctuations ($\approx$700 Pa)	10
spread of M in each layer	5
	18
Accuracy of measurement of drift time:	
internal resolution	40
inaccuracy of drift-time–coordinate relation	20
	45
Resolution of the drift chamber	50–55

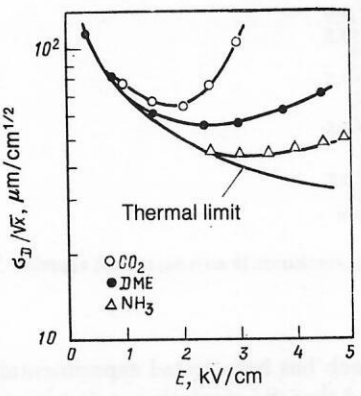

FIG. 12. The dependence $\sigma_D(E)/\sqrt{x}$ in cool gases.[32]

the world, great efforts are being made to improve the spatial resolution of drift chambers. The main advantage of high-precision drift chambers compared with semiconductor microstrip detectors is their low cost and the possibility of construction of large drift chambers.

In order to achieve a high accuracy in the drift chambers, one uses: 1) "cool" gases; 2) a high pressure; 3) selection of short track sections; 4) measurement of the cluster drift time; 5) multiple measurement of track coordinates.

In high-precision chambers, a combination of these measures is usually employed.

Cool gases

The main contribution to the spatial resolution of a drift chamber is made by diffusion of the electrons in the gas. In high-precision chambers, it is necessary to use gases with a low diffusion coefficient. As we have already said, such are the cool gases: CO_2, NH_3, dimethylether (C_2H_6O), methylal [$(CH_3O)_2CH_2$], and isobutane (iso-C_4H_{10}). These gases have a large momentum transfer cross section $\sigma_m \approx 10^{-14} - 10^{-13}$ cm^2 (Ref. 20), and therefore the electrons in them remain thermal even at a high electric field strength, and their characteristic energy is $\varepsilon_k = kT$. Because of this, their drift velocity is low (a few mm/μsec) even at $E \approx 1$ kV/cm, and σ_D is close to the thermal limit (11). The dependence $\sigma_D(E)$ in cool gases is shown in Fig. 12. By using cool gases in a drift chamber one can improve its spatial resolution by ~ 2 times.

The use of slow electron drift in a chamber filled with dimethylether at atmospheric pressure made it possible[31] to achieve a resolution of $\sigma_x/\sqrt{x} \approx 16$ μm/cm$^{1/2}$.[31]

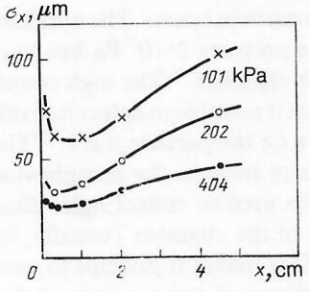

FIG. 13. Dependence of spatial resolution σ_x on the drift length and pressure[30] in mixture of 75% C_3H_8 and 25% C_2H_4.

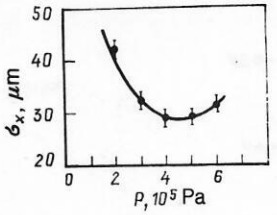

FIG. 14. Dependence of σ_x on the CO_2 pressure for drift length $x = 8$ mm.[32]

Higher pressure

The spatial resolution can be improved by raising the pressure if one ensures a corresponding increase of E, so that $E/P = \text{const}$. Then from (8)–(10)

$$\sigma_D = \sqrt{\frac{2D(E)x}{\mu E}} = \sqrt{\frac{2kT}{eE/P}}\sqrt{\frac{x}{P}}. \qquad (15)$$

The dependence $\sigma_x(x)$ for different gas pressures is shown in Fig. 13. The dependence of σ_x on the CO_2 pressure measured by the group at the Moscow Engineering Physics Institute[32] is shown in Fig. 14.

In a drift chamber filled with cool gas at pressure $(4–5)\cdot 10^5$ Pa one can achieve a spatial resolution of $\sigma_x/\sqrt{x} \approx 25–30$ μm/cm$^{1/2}$ and a two-track resolution (with efficiency 70%) of $x_{12} \approx 100$ μm.[32] At superhigh pressures, for example, $P = 3\cdot 10^7$ Pa, the same group achieved a resolution of $\sigma_x/\sqrt{x} = 10–15$ μm/cm$^{1/2}$

Selection of short track sections

The value of σ_s [see (3)] can be reduced if one uses for coordinate determination only a small section of the track nearest the signal wire. Then the difference between the times of arrival of the electrons at the signal wire can be reduced to a minimum. The selection of the necessary section of the track can be done mechanically (Fig. 15a) or by means of an electric field (Fig. 15b). For example, in Ref. 32 the first method was used, a slit of width 0.9 mm being chosen to ensure $\sigma_s \leqslant \sigma_D$, for $x = 2$ mm. Such a method improves the spatial resolution but raises the requirements on the electronics.

Measurement of cluster drift time

The most radical approach to the attainment of the limiting spatial accuracy in drift chambers has been pro-

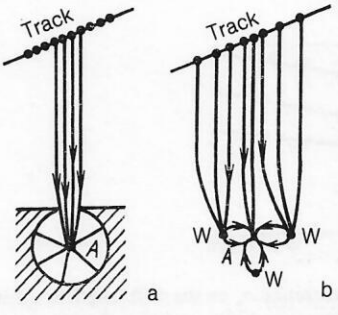

FIG. 15. Selection of part of the particle trajectory: a) by mechanical limitation; b) by electric field; A is the anode and W are field-shaping wires.

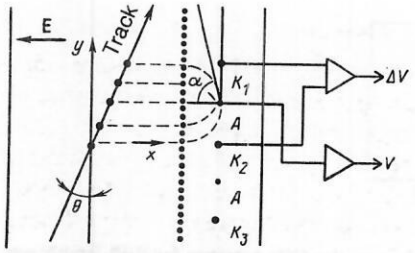

FIG. 16. Principle of measurement of cluster coordinates in a drift chamber.

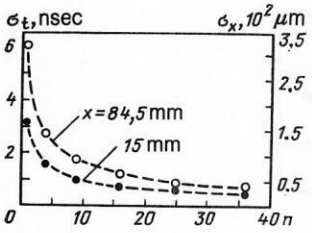

FIG. 18. Spatial σ_x and time σ_t, resolution in an n-layer drift chamber.[36]

posed by Walenta *et al.*[33] The method is based on determination of the coordinate of each cluster, the track being reconstructed by drawing a straight line through the resulting points. The accuracy in the determination of the track coordinate is then

$$\sigma_x = \sigma_1/\sqrt{N_c}, \tag{16}$$

where N_c is the number of detected clusters on the measured section of the track. Thus, in the standard gas mixture, for which $N_c \approx 30/\text{cm}^{-1}$, one can theoretically achieve an improvement of the spatial resolution by 3–5 times.

The principle of operation of a drift chamber for measurement of the cluster coordinates is shown in Fig. 16. One measures the drift time of the clusters, and also the angle α of incidence of the clusters on the signal wire. The angle α corresponds to the position of the cluster along the track of the particle. It is determined by comparing the charges induced on the electrodes K_1 and K_2, which are placed a small distance from the signal wire (A). By this method, Walenta *et al.*[33] determined the angle α to an accuracy $\pm 2.3°$. Figure 17 shows the spatial resolution obtained in a chamber with measurement of the cluster drift time in an 80% CO_2 + 20 % iso-C_4H_{10} mixture. The two-track resolution in such a chamber is $x_{12} \approx 0.2$ mm.[8]

To measure the cluster drift time, one needs fast electronics with dead time ≈ 15 nsec.[5,34,35] An important aspect of such electronics is the need to shape signals and eliminate long tails of them.

Multiple measurement of track coordinates

High-precision localization of the trajectories of high-energy particles, for which a small amount of multiple scattering is characteristic, can be achieved by multiple measurement of the trajectory coordinates in a multilayer chamber. Such an approach has been tested experimentally,[36] and it has been found that the resolution $\sigma_x(n)$ is improved in accordance with the number n of points of measurement: $\sigma_x(n) = \sigma_x/\sqrt{n}$. The dependence $\sigma_x(n)$ is shown in Fig. 18. The principle of multiple measurement of the coordinates is used in high-precision drift chambers (for example, in the micro-jet chamber of Va'vra *et al.*[37] or in Ref. 38).

For many large colliders and experiments with a fixed target, vertex detectors based on high-precision drift chambers have been developed (Refs. 32, 33, and 36–40). These employ a combination of the methods listed for improving the spatial resolution, the aim being to achieve a resolution of $\sigma_x/\sqrt{x} \approx 40$–$50$ μm/cm$^{1/2}$ and $x_{12} \approx 500$ μm at pressure 10^5 Pa and $\sigma_x/\sqrt{x} \approx 20$–$30$ μm/cm$^{1/2}$ and $x_{12} = 100$–200 μm at a higher pressure. (*Note added in proof*: After this review had been completed, the interesting paper of Ref. 41 on high-precision drift chambers was published.)

This class of high-precision chambers also includes narrow-gap drift chambers and scintillating chambers. Both types are designed for operation in high particle fluxes.

Narrow-gap drift chambers

Narrow-gap drift chambers[42–44] are distinguished by a short electron drift length (< 10 mm) and the absence of field-shaping electrodes (see Fig. 2b). If the conditions of operation mentioned above are observed, a high spatial resolution is attained in them. A shortcoming of these chambers[42,43] is the high number of channels of the electronics.

Scintillating drift chambers

In scintillating drift chambers,[45–48] the time of arrival of the electrons at the anode is determined by means of the photons that are produced by the gas luminescence in the process of gas multiplication. The photons are usually detected by means of photomultipliers. The main advantage of such chambers is their high counting rate and the possibility of working them at a low gas multiplication; this makes it possible to use them in intense particle beams. The excellent spatial resolution of 16 μm at pressure $2 \cdot 10^5$ Pa has been achieved in a scintillating drift chamber.[46] The high counting rate of such chambers makes it possible to detect individual primary ionization clusters on the particle track.[48] The shortcomings of these chambers include the complicated construction resulting from the need to collect light effectively from the complete area of the chamber (usually, by means of photomultipliers). This makes it difficult to construct large chambers, and hitherto no large system of this kind has been operated.[8]

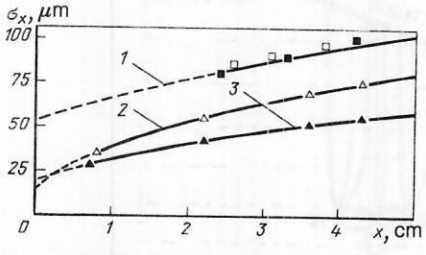

FIG. 17. Dependence of spatial resolution σ_x on the drift length in a drift chamber when cluster coordinates are being measured[8]; the curves correspond to $\sigma_x = \sqrt{\sigma_D^2 x + \sigma_A^2}$. $\sigma_D = 40$ μm/cm$^{1/2}$, $\sigma_A = 54$ μm; 2) $\sigma_D = 36$ μm/cm$^{1/2}$, $\sigma_A = 14$ μm; 3) $\sigma_D = 25$ μm/cm$^{1/2}$, $\sigma_A = 19$ μm.

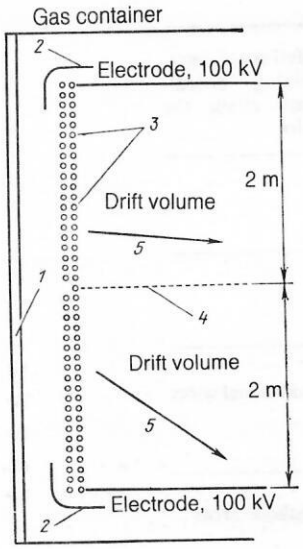

FIG. 19. Arrangement of the multilayer drift chamber ISIS[49]: 1) mylar window; 2) screen; 3) field-shaping electrodes; 4) signal wires; 5) track.

3. MULTILAYER DRIFT CHAMBERS

A multilayer drift chamber contains a large volume of gas with a homogeneous electric field in which electrons from particle tracks diffuse to a system of many signal wires, where their time of arrival is determined (Fig. 19). The space above each signal wire is called a layer. Multilayer drift chambers are also called pictorial chambers or time projection chambers. They provide a three-dimensional reconstruction of events with high multiplicity and make it possible to identify secondary charged particles on the basis of multiple measurement of the ionization energy losses.[9] The quality of the image of the particle tracks in such a chamber is very high, as is illustrated by Fig. 20.

The idea of creating large multilayer drift chambers arose at the beginning of the seventies.[50,51] The first chambers [ISIS Ref. 52, TPC (Ref. 53), JADE (Ref. 54), UA-1 (Ref. 55)] were commissioned at the beginning of the eighties.

There are two main types of multilayer drift chamber: flat and cylindrical.

Planar multilayer drift chambers

Planar chambers are usually employed as external identifiers of relativistic charged particles in magnetic spectrometers with a fixed target, for example, the chamber ISIS (Refs. 52 and 56) in the European Hybrid Spectrometer at CERN, CRISIS (Ref. 57) at Batavia, and ASTRON,[58] which is being developed at the Institute of High Energy Physics at Serpukhov. They are also used as vertex detectors, for example, in the facility of the European Muon Collaboration (EMC)[59] at CERN, the IKS chamber[60] in the MARS facility at Dubna, or the time projection chamber (TPC)[61] in the OMEGA facility at CERN. Multilayer drift chambers are also used to measure the ranges of heavy ions.[62] The basic parameters of a number of planar multilayer chambers are given in Table II.

The spatial resolution σ_x (the coordinate $x \| E$ is determined by measuring the electron drift time) is governed by the drift length. The coordinate along the wire is determined in different ways, and therefore the rms error σ_y in its measurement varies in wide ranges. The two-track resolution x_{12} is determined in the first place by the signal length.

Cylindrical multilayer drift chambers

Cylindrical chambers, placed in a magnetic field, permit accurate determination of emission angles and the measurement of the momenta of charged particles in collider experiments. They are usually called central detectors. Because detectors in colliding-beam experiments must be very compact, there is a strong limitation on the radial dimensions of a central detector, and to achieve the necessary momentum resolution it is necessary to ensure a high accuracy of measurement of the particle trajectories.

There are various types of construction, and there are currently four main variants of such chambers:

1) TPC, with axial drift of the electrons;

2) JET, with azimuthal drift of the electrons (with small drift length);

3) CDC, chambers with the "classical" configuration of wires in cylindrical layers;

4) WDC, cylindrical chambers divided into flat wide-gap drift chambers.

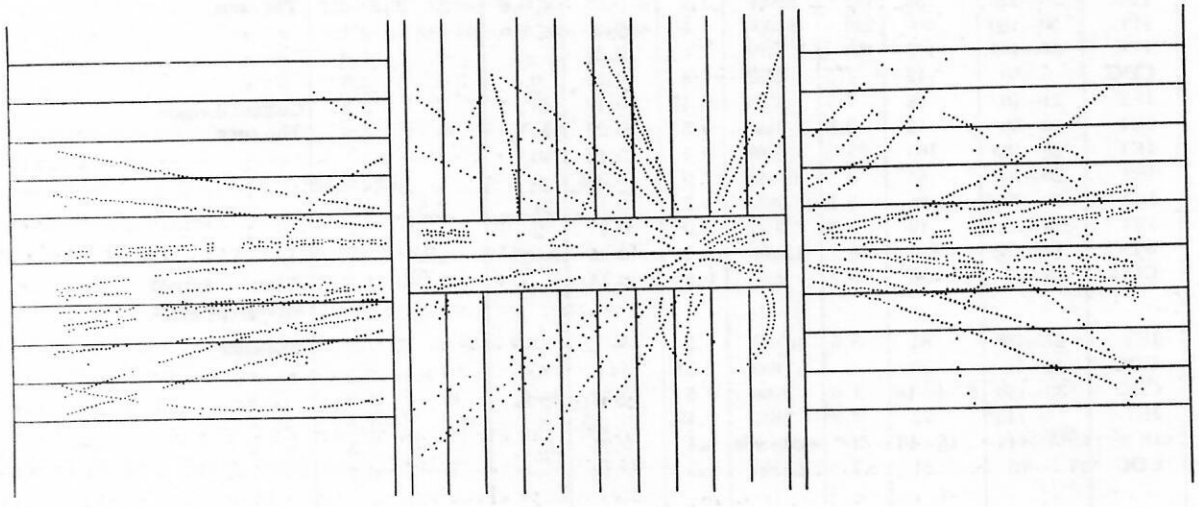

FIG. 20. Multitrack $p\bar{p}$ event at energy 540 GeV detected in the multilayer drift chamber of the UA-1 facility.[55]

TABLE II. Basic parameters and spatial resolution of planar multilayer drift chambers (1985).

Facility	Chamber length, cm	Number of layers	Maximal drift length, cm	Length of wire, cm	Number of electronics channels	Magnetic induction, T	σ_x, mm	σ_y, mm	x_{12}, mm	Method of determining coordinate along the wire
ISIS	510	320	200	200	320	—	<3	—	12	—
CRISIS	300	192	25.4	103	384	—	<2	—	10—12	—
ACTPOH	450	250	50	100	330	—	$\leqslant 0.5$	7	8—10	Additional wires
EMC	155	325	30	60—145	6260	1.5	$\leqslant 1$	0.25	20	Cathode areas
IKS	160	80	35	85	240	1.5	$\leqslant 0.5$	$\leqslant 1$	8	Delay lines
OMEGA — TPC	20	16	16	40	224	1.2	0.25	—	—	Cathode areas

These designations of the cylindrical multilayer drift chambers are used in Table III, which gives their basic parameters. A more detailed description of the types of such chambers can be found, for example, in Refs. 9 and 63.

Large time projection chambers are used in the PEP-4–TPC facility[51,53,64] in the PEP colliding e^+e^- beams at SLAC and are being developed for the detectors DELPHI (Ref. 65) and ALEPH (Ref. 66), which will be used in the e^+e^- beams of LEP at CERN and the detector TOPAZ (Ref. 67) in the e^+e^- beams of TRISTAN. These chambers are distinguished by the long electron drift length, which determines the accuracy σ_y of measurement of the coordi-

TABLE III. Basic parameters and spatial resolution of large cylindrical multilayer drift chambers (1986).

Facility	Type of chamber	Internal–external radius, cm	Numbers of layers	Maximal drift length, cm	Number of electronics channels	Magnetic induction, T	$\sigma_{r\varphi}$, mm	σ_y, mm	x_{12}, mm (deg)	σ_p/p^2, % GeV$^2/c^2$	Method of determining coordinate along signal wire
PEP-4	TPC	20—100	183	100	13 824	1.45	0.16	0.34	10—20	3.7	Cathode areas
DELPHI	TPC	30—120	188	140	22 000	1.2	$\leqslant 0.25$	$\leqslant 0.8$	<20	0.5—0.7	The same
ALEPH	TPC	30—180	400	220	50 000	1.5	$\leqslant 0.2$	$\leqslant 1.5$	12—18	0.12	» »
TOPAZ	TPC	36—109	175	150	5496	—	0.23	—	—	1.0	» »
CELLO	CDC	5—60	12	7.5	6432	1.3	0.21	0.4	3.5°	2.0	» »
JADE	JET	21—79	48	7.5	1536	0.45	0.16	13	7	2.2	Current division
AFS	JET	20—80	42	2.8	3444	0.5	0.22	14	40	2.0	The same
OPAL	JET	25—185	160	25	7680	0.4	0.12	40	2		» »
SLD	JET	20—100	80	3	11 648	1.0	0.055	9	1	0.2—0.55	» »
H1	JET	20—79.5	64	5.1	5120	1.2	0.1	24	2.5	0.3	» »
KMД-2	JET	2.5—29.5	19	2.8	1024	2.0	0.1	2	—	—	» »
UA-1	WDC	10—122	~ 110	18	12 200	0.7	0.25	8—25	2.5	—	» »
ARGUS	CDC	15—85	36	9.5	5940	0.8	0.15		9	1.2	Wires turned through an angle
CDF	JET	27—138	84	3.5	10 080	1.5	—	—	<1	—	The same
MAC	CDC	12—45	20	—	833	0.57	—	4	—	6.5	» »
TASSO	CDC	32—130	8+4+16	1.6	3060	0.5	0.22	3—4	16	1.0	» »
MARK-II/SLC	JET	23—145	72	3.3	5832	0.45	0.175	4	$\leqslant 3$	1.5	» »
MARK-III	JET	14—114	15+18	3	416+1584	0.4	0.25	15	—	1.5	» »
CLEO-II	CDC	17.5—95	51	7	12 240	1.5	0.18	—	—	0.7	» »

nate y along the chamber axis. The azimuthal coordinate is usually measured with high accuracy ($\sigma_{r\varphi} \approx 0.2$ mm).

Chambers of the JET type are designed for the detection of events with a high track multiplicity under conditions of a high particle flux. In them, the electrons drift a short distance in the azimuthal direction, and this permits a good spatial resolution of $\sigma_{r\varphi} \approx 0.1$–$0.25$ mm. In these chambers, the wires are stretched along the chamber axis, and therefore the coordinate y is determined with a low accuracy, $\sigma_y \approx 15$–20 mm. Such chambers are used in the JADE facility[63,68] in the e^+e^- beams of PETRA at DESY, in the AFS facility[69] in the ISR $p\bar{p}$ collider at CERN, in the MARK-III facility in the e^+e^- beams of PEP at SLAC and are being developed for the OPAL facility[71] of the e^+e^- collider LEP at CERN and the CDF facility[72] in the $p\bar{p}$ beams at Fermilab, the SLD facility[73] in the e^+e^- linear collider SLC at SLAC, the H1 facility in the ep collider HERA at DESY,[74] the KMD facility[75] in the e^+e^- collider VÉPP-2M, and the MARK-II/SLC facility[76] the e^+e^- collider SLC at SLAC.

The cylindrical multilayer drift chambers of classical construction (CDCs) are distinguished by a short drift length and, accordingly, good resolution $\sigma_{r\varphi} \approx 0.15$–$0.25$ mm. The chambers of this type usually do not have many layers (20–40). They are used, for example, in the facilities ARGUS (Ref. 77), TASSO (Ref. 78), and CELLO (Ref. 79) in the e^+e^- beams at DESY and in the facilities MAC (Ref. 80) and CLEO-II (Ref. 81) in the e^+e^- collider CESR at Cornell University.

The cylindrical multilayer drift chamber[55] of the UA-1 facility in the $p\bar{p}$ collider SPS at CERN is divided by planes of wires into rectangular sections (WDC type). Such a structure of the chamber is advantageous for use in a dipole-magnet facility.

Table III also gives the two-track resolution x_{12} in the direction of the electron drift and the particle-momentum resolution σ_p/p^2.

Electronics time-to-digital converter (TDC)

The electronics for multilayer drift chambers is distinguished by its ability to detect a series of signals coming in rapid succession from the chamber. The electronics must measure with high accuracy the time of arrival of each of the signals, and, in ionization measurements, their amplitude as well.

The signal arrival time is measured by means of a multiple time–digital converter[82–85] with the following basic parameters: measured time interval 2–16 μsec, accuracy of time measurement 1–4 nsec, dead time 32–64 nsec, maximal number of detected signals 8–256.

The signal amplitude is measured by means of a fully parallel, or "flash," analog-to-digital converter (ADC)[86–88] with the following basic properties: resolution 6–8 bits, dead time 10–100 nsec, maximal number of detected signals 128–1024.

The electronics for multilayer drift chambers is described in more detail in Ref. 9, for example.

Measurement of coordinate along signal wires

In large multilayer drift chambers spatial reconstruction of tracks is often necessary. Therefore, besides good spatial resolution in the direction of the electron drift it is also necessary to ensure measurement of the coordinate along the signal wires with good resolution. In planar multilayer drift chambers the coordinate along the wires (y) is not always measured. Depending on the method of measuring the coordinates, multilayer drift chambers can be divided into several classes. In chambers of the TPC type (in the facilities PEP-4, DELPHI, ALEPH, and TOPAZ; see Table III), the azimuthal coordinate (r, φ) is determined by measuring the centroid of the signals induced on cathode strips. The coordinate along the chamber axis (y) is determined from the electron drift time. In chambers of JET type (in the facilities JADE, AFS, OPAL, CDF, MARK-III, SLD, H1 CMD-2 and also in the other cylindrical multilayer drift chambers listed in Table III), the coordinate (r, φ) is measured from the drift time, and the coordinate y (along the wires in these chambers) is measured in various ways, which are listed below. This task is not one of the easiest. There are several methods for determining the coordinate along the signal wire.

a) Current division

This method, proposed by Charpak, is based on measurement of the currents I_1 and I_2 at the two ends of the signal wire. The currents are divided in accordance with the resistances R_1 and R_2 of the sections of the wire on the two sides of the electron avalanche:

$$I_1/I_2 = R_2/R_1 = (L_w - y)/y, \tag{17}$$

where y is the distance from the beginning of the wire to the electron avalanche on the wire, L_w is the length of the wire, and ρ_w is its resistivity. The coordinate y along the wire is

$$y = L_w I_2/(I_1 + I_2). \tag{18}$$

The current-division method is often used in drift chambers, and it has been well studied.[89] The accuracy in the measurement of the coordinate is determined by the signal-to-noise ratio, and one therefore uses a wire with high resistivity ρ_w (generally, stainless steel). The spatial resolution depends on the capacitance C_w of the wire and the charge Q collected on it[89]:

$$\Delta y/y = 2.54 \sqrt{kTC_w}/Q. \tag{19}$$

The limiting error of the method is low: $\Delta y/y \approx 1\%$. The use of this method also requires a relatively high gas multiplication ($M \approx 10^5$); in ionization measurements, this is undesirable. The current-division method is usually employed in chambers of the JET type (see Table III).

b) Measurement of the centroid of the induced charge on the cathodes

This method is often used in proportional and drift chambers (in Tables II and III, these are called "cathode areas"). The chamber cathodes are made in the form of strips or areas (Fig. 21) of width 5–10 mm. On each strip i the induced charge Q_i is measured, and the coordinate of the electron avalanche on the wire is calculated:

$$y = \sum_i Q_i y_i / \sum_i Q_i. \tag{20}$$

This method has been well studied and is often used (Refs. 8, 64, and 90–92), since it ensures a high spatial resolution (σ_y

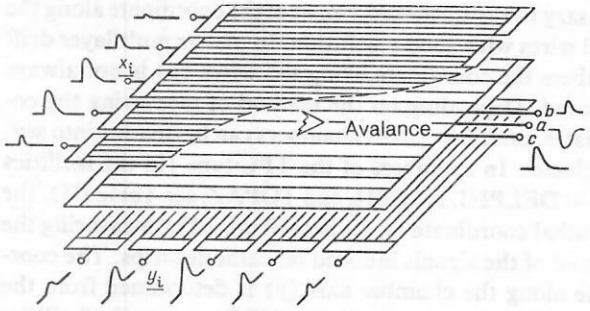

FIG. 21. Arrangement of a chamber for measuring the centroid of induced charge on the cathodes.[8]

$= 20$–$30\ \mu$m has been achieved). In large drift chambers, the limiting resolution is not attained because of the influence of diffusion, inclination of the tracks, etc., but in large chambers of the TPC type a resolution 100–200 μm is obtained. A shortcoming of this method is the large number of channels (see Table III) and the use of costly electronics for measurement of the signal amplitudes. The method using measurement of the centroid of the induced charge is usually employed in TPC chambers to determine the azimuthal coordinate. The spatial resolution $\sigma_{r\varphi}$ given in Table III was obtained by this method.

c) Use of a delay line

A delay line can be used as a cathode. The signal induced on it propagates in both directions along the wire with known velocity. The coordinate of the electron avalanche on the wire is determined from the difference between the times of arrival of the signals on the anode wire and at the end of the delay line. It is better to receive signals at both ends of the delay line, and in this case one can detect several particles passing simultaneously through the drift chamber.[60] Delay lines are often used in drift chambers (Refs. 5, 89, and 93–95). They are placed quite near the signal wires, and therefore they must contain the minimal amount of material. This has the consequence that the delay obtained by means of them is short, i.e., the signal passes rapidly through the delay line (the signal propagation velocity is about 10 mm/nsec). Using fast delay lines, one can achieve an accuracy of $\Delta y \approx 5$ mm if the delay line has length 1–1.5 m. In slower delay lines (velocity 0.3–0.5 mm/nsec), a better spatial resolution $\sigma_y \leqslant 0.1$ mm can be achieved with a delay line of length 20 cm.[93]

d) Rotation of the plane of signal wires through a small angle

The rotation method is used in cylindrical drift chambers (see Table III), the signal wires in some layers being turned through a small angle α_s (4–6°) to the chamber axis (Fig. 22). The coordinate y along the wire is determined to accuracy

$$\sigma_y = \sigma_{r\varphi}/\tan\alpha_s. \tag{21}$$

A typical value is $\sigma_y = 20\sigma_{r\varphi}$, i.e., $\sigma_y \approx 4$–5 mm.[39]

e) Use of wires or strips perpendicular to the signal wires

This method is used in the ASTRON facility,[58] where it is used to detect some of the electrons from the particle tracks (designated in Table II as "additional wires"). It ensures a spatial resolution equal to the distance between the additional wires (in ASTRON, $\Delta y = 15$ mm). Another similar method consists of using strips of trapezoidal form along the wires. The amplitude of the induced charge on the strip corresponds to the position of the electron shower along the wire.[96–98]

Right–left ambiguity

Right–left ambiguity is an inconvenient property of drift chambers. To establish whether the electrons arrive on the wire from the right or the left, the following additional measures are taken:

1. Instead of a single signal wire, two, separated by a small distance (less than 1 mm), are used.

2. Two drift chambers situated near each other are shifted relative to each other by half the distance between the signal wires.

3. In multilayer chambers of the JET type, the even wires are shifted in one direction and the odd wires in the opposite direction from the central plane. In the JADE chamber, this shift is 0.15 mm (Ref. 68), and in the chamber AFS it is 0.4 mm.[69]

4. The induced charge on additional electrodes situated on the sides of the signal wire is measured. The charge will be greater on the electrode situated in the part of the chamber through which the particle passed.[33]

Multilayer drift chambers in a magnetic field

In a magnetic field, the electron drift velocity w_M and the diffusion coefficient D_M are reduced:

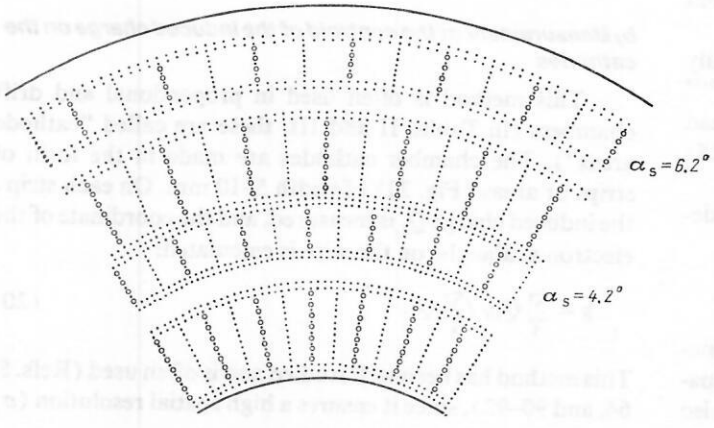

FIG. 22. Schematic arrangement of module of a cylindrical drift chamber with layers of wires turned through an angle α_s.

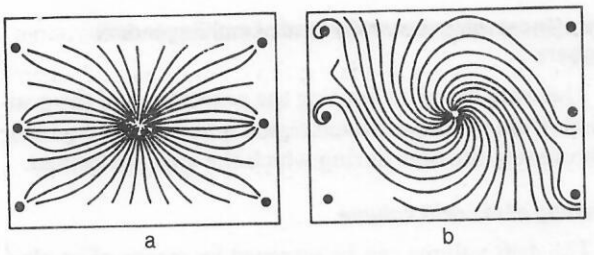

FIG. 23. Trajectories of electrons in the drift chamber CELLO: a) $B = 0$; b) $B = 1.5$ T.[14]

$$w_M = w_d/\sqrt{1+w_M^2\tau_M^2}; \quad (22)$$

$$D_M = D(E)/(1+\omega_M^2/\nu_e^2), \quad (23)$$

where $\omega_M = eH/m_e$ is the Larmor frequency, $\tau_M(E, H)$ is the mean free time of the electron in the crossed electric and magnetic fields, and ν_e is the frequency of electron collisions with the atoms of the gas. The electrons move at angle α_M to the direction of the electric field gradient:

$$\tan\alpha_M = \omega_M\tau_M. \quad (24)$$

Therefore, their trajectories are not perpendicular to the plane of the signal wires, as illustrated in Fig. 9 for the example of the drift chamber JADE. In chambers with a different configuration of the electrons, the addition of a magnetic field leads to an even more significant distortion of the electron trajectories (Fig. 23), and in this case it is difficult to recover the coordinate of the particle track from the measured drift time. Therefore, when the drift chamber is operated in a magnetic field it is necessary to employ additional measures to compensate these effects. In planar drift chambers with a distributed potential (shown schematically in Fig. 2c), the electric field configuration is changed in such a way as to compensate the influence of the magnetic field on the electron trajectories. Such shifting of the direction of the electric field is achieved by applying equal potentials to a pair of wires whose axes lie on a line at an angle α_M to the plane of the signal wires.[5,7] It is proposed to use this principle of compensating the magnetic field by the electric field in the large cylindrical chambers for the LEP colliding beams at CERN.[15] The modules of the chambers of JET type are arranged "along a spiral," and this has the consequence that in the magnetic field of the solenoid the electrons drift in the direction perpendicular to the plane of the signal wires.

The most favorable situation arises in the drift chambers in which $\mathbf{E}\|\mathbf{B}$ and the trajectories of the electrons are hardly changed when the magnetic field is present. This condition is satisfied in chambers of the type TPC placed in the magnetic field of the solenoid, and this is one of their main advantages.

For a drift chamber operated in a magnetic field it is desirable to choose special gas mixtures in which the angle of deflection of the electron trajectories in the magnetic field, α_M, is small. Mixtures based on cool gases have this property.

The expression (24) can be rewritten in the form

$$\tan\alpha_M = eH/m_e n_a v_e \sigma_e, \quad (25)$$

where v_e is the velocity of the electrons, and σ_e is the cross section of their elastic collisions with atoms of the gas. In cool gases, the elastic cross section σ_e is large, and therefore $\tan\alpha_M \ll 1$ (≈ 0.03 in CO_2; ≈ 0.01 in NH_3 and in C_2H_5OH for $B = 0.5$ T (Ref. 30)). The results of measurements of the angle α_M as a function of the electric and magnetic field strengths in mixtures of carbon dioxide gas with argon and isobutane are given in Table IV. In mixtures with a high CO_2 concentration, the angle α_M is almost an order of magnitude smaller than in the "ordinary" mixtures used in drift chambers.

The transverse diffusion coefficient D in the presence of a magnetic field is appreciably reduced, above all in "fast" gases. It is interesting to note that in a magnetic field a decrease of the longitudinal diffusion coefficient D_L is not observed.[99]

4. COUNTING RATE OF MULTILAYER DRIFT CHAMBERS

Restrictions on the counting rate

The counting rate of multilayer drift chambers is restricted by three main factors: the electron collection time, the signal duration, and the accumulation of space charge in the drift volume.

Electron collection time

The electron collection time is determined by the electron drift length. In chambers with a large drift volume, it can be appreciable; for example, in the chamber ISIS with drift length up to 2 m it reaches 50 μsec. Such chambers (ISIS, CRISIS, EPI) are used as external identifiers after bubble chambers, which are also not able to withstand heavy loads. Therefore, the particle flux density in these experiments does not exceed 10^4 particles$\cdot$m$^{-2}\cdot$sec^{-1}.

In multilayer drift chambers used in colliding beams the

TABLE IV. Drift angle α_M of electrons in a magnetic field in different gas mixtures.[100]

CO_2, %	iso-C_4H_{10}, %	Ar, %	E, kV/cm	B, T	α_M, deg	
					Measurement	Calculation
95	5	—	0.4	0.5	1.0	2.0
95	5	—	0.66	0.5	1.3	2.1
95	5	—	0.8	0.5	1.2	2.1
95	5	—	2.4	0.5	2.5	2.2
95	5	—	2.4	1.0	5.2	4.4
20	—	80	1.0	0.5	14.1	12.5
20	—	80	1.0	0.925	23.8	22.2
90	—	10	0.6	0.5	0.45	2.2

collection time is chosen to be less than the time of revolution of a particle bunch in the storage ring, for example, less than 4.6 μsec in the SPS at CERN and less than 22.5 μsec in LEP. It can be seen from this that the restrictions on the collection time in these storage rings are not stringent. In chambers of the JET type with a collection time 1–2 μsec, the required condition is readily satisfied. More serious problems can arise in the time projection chambers, for which, with a drift length of 1 m, the collection time is of order 20 μsec.

It should be noted that one can also work at loads for which several beam particles pass through the chamber during the electron collection time. Their tracks can be readily eliminated during analysis, since they do not pass through the interaction vertex. The elimination of such tracks is also facilitated by fast coordinate detectors, for example, proportional chambers, placed in front of and behind a multilayer drift chamber.

Signal duration

In drift chambers used to measure ionization the signal duration is 100–150 nsec, and this gives a restriction on the particle flux of $\sim 10^6$ particle/sec per wire.

Influence of space charge on reconstruction of the particle track

The accumulation of space charge in the chamber gives rise to the most serious restrictions on the admissible particle flux. The number N_+ of positive ions produced in the process of gas multiplication near the signal wire is given by the expression

$$N_+ = \phi P M n_e l \sin^{-1}\theta, \tag{26}$$

where ϕ is the number of charged particles detected by one wire per unit time, M is the gas amplification coefficient, n_e is the number of electrons on a part of the track of length l, and θ is the angle of inclination of the track to the plane of the signal wires. In large chambers, the ion collection time τ_+ may reach fractions of a second. Thus, in a volume V within the chamber a positive charge accumulates with density

$$\rho_+ = eN_+\eta_+\tau_+/V, \tag{27}$$

where η_+ is the efficiency of penetration of the ions from the proportional region to the drift region. The charge in volume V with coordinates x, y, z within the chamber leads to a change in the electric field strength:

$$\delta E_x = \frac{\rho_+ x}{3\varepsilon};\ \delta E_y = \frac{\rho_+ y}{3\varepsilon};\ \delta E_z = \frac{\rho_+ z}{3\varepsilon}, \tag{28}$$

where ε is the gas permittivity. This, in its turn, leads to changes in the drift velocity w_d and the direction of motion of the electrons, and these are appreciable if the space charge exceeds the charge q_w per unit length of the wire[52]:

$$\int \rho_+(x)dx > 10^{-3} q_w. \tag{29}$$

If ρ_+ increases still further, then serious deformations of the tracks are observed. For example, in the chamber ISIS the allowed charge density $\rho_+ = 5$ nC/m^3 corresponds to a particle flux density not greater than $1.3 \cdot 10^3$ m$^{-2}\cdot$sec^{-1}.

Ways of increasing the useful load of multilayer drift chambers

These are based on limiting the penetration of the positive ions from the proportional region into the drift region or on shortening the time during which the ions are formed.

Screening of the drift volume

The drift volume can be screened by means of an electric gate that does not permit electrons from the drift volume to enter the proportional volume or positive ions to move in the opposite direction. In the normal state, the gate is shut and is opened following a trigger pulse, when it is necessary to detect the useful event. The gate opening time must be short (a few hundred nanoseconds), so as to prevent loss of some of the electrons, which enter the proportional volume with velocity ≈ 5 cm/μsec.

Methods of controlling chambers of the time projection type by means of gates are becoming more and more widespread [91,101–104] Two types of gate are used. In the first, the drift volume is separated from the proportional volume by two grids separated by a short distance to which a potential is applied of such magnitude that in the case of an open gate the electrons freely pass through it. The gate is closed by reversing the polarity on the outer grid (the one further from the proportional volume) relative to the inner grid. In this case, the electrons cannot drift through the gate, and they collect on the outer grid.

The other type of gate (Fig. 24) has in the open state a potential on the outer grid that permits the electrons to pass freely through it. In the closed state, a positive voltage $+U_g$ is applied to the even wires and a negative voltage $-U_g$ to the odd wires. The lines of force created in this manner between neighboring wires block the passage of the electrons through the grid.

The second type of gate is more advantageous. A voltage $U_g = 100$–200 V must be applied to the first type of gate, and the gate opening time for it is longer than 1 μsec; for the second type, $U_g = 20$–50 V and the opening time is about 200 nsec.[101,104] For the first type of gate, the pickups on the amplifiers are also much greater. In the presence of a strong magnetic field, the voltage U_g must be increased by 2–3 times.[104] Well adjusted gates operate very effectively, and

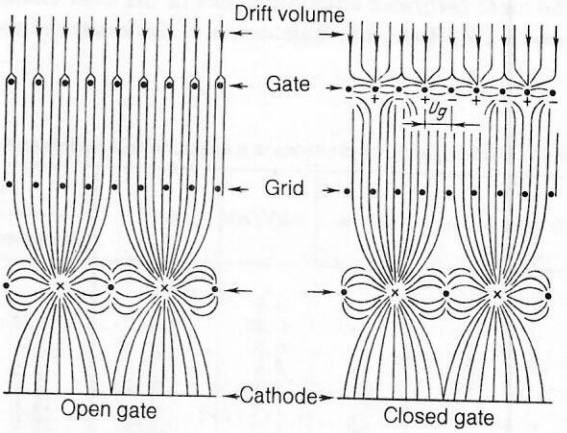

FIG. 24. Principle of gate in a time projection chamber (the crosses represent the anode wires).

they enable the load on the drift chambers to be greatly increased (by about two order of magnitude).[103,104]

Insensitive zone in the region of the beam

In the region through which the beam passes, a small insensitive zone is created, from which electrons do not emerge. This method is employed only in multilayer drift chambers operating in facilities with a fixed target (in cylindrical multilayer chambers in storage rings, the beam passes through the vacuum tube). An insensitive zone can be created in various ways:

a) In the EPI chamber[102] the signal wires are covered by a thin layer of glass where the beam passes.

b) In the multilayer drift chamber in the European Muon Spectrometer at CERN the beam passes through a thin tube.[59]

c) Between the beam and signal wires one can span a thin metallic foil of width equal to the beam width.[60]

Usually, about 10% of the beam particles interact in the target, so that after the creation of an insensitive region around the beam the useful load can be increased by about an order of magnitude.

Pulsed anode voltage

To increase the useful load, the anode voltage (usually 2–3 kV) is reduced by about 500 V during the time when there are no triggers. This method is not so good as the use of gates, since large changes in the voltage give rise to pickup on the amplifier during the switching time. The pulsed regime can be used only if the chamber works in conjunction with a slow device, for example, a bubble chamber with cycling rate less than 10 Hz. The anode voltage can also be switched off during the time of transmission of information to a computer. A pulsed regime was, in particular, used in the chamber ISIS, where the anode voltage was switched off only for 5% of the time; this made it possible to increase the allowed particle flux density from $1.3 \cdot 10^3$ to $2.5 \cdot 10^4$ $m^{-2} \cdot sec^{-1}$.

Use of minimal gas multiplication

The chamber load is inversely proportional to the gas multiplication. On the other hand, for good spatial resolution it is necessary to have sufficiently large signal amplitudes, and therefore an optimal gas multiplication must be chosen.

Reduction of the drift length

In the choice of a suitable type of chamber, it is necessary to take into account the maximal particle flux in the facility. In high particle fluxes, chambers with short drift length (for example, chambers of the JET type) work well. The allowed load is inversely proportional to the drift length.

Field-shaping electrodes in the drift volume

The influence of the space charge in the drift volume can be significantly reduced by introducing field-shaping electrodes. A voltage corresponding to a linearly decreasing potential is applied to these electrodes (which are in the form of wires). They compensate the influence of the charge of the positive ions on the motion of the electrons. The use of this method in the TPC chamber in the OMEGA facility at CERN made it possible to increase the useful load by about an order of magnitude.[105]

The use of the measures listed above makes it possible to increase appreciably the load on multilayer drift chambers. These measures are usually combined, and this makes it possible to use the chambers in particle fluxes of high intensity.

Calibration of large chambers

In large chambers with a long drift length it is necessary to know and control the velocity and direction of the electron drift with high accuracy. For example, for a required spatial resolution $\sigma_{r\varphi} \approx 100\,\mu$m in a TPC chamber with drift length 1 m the speed and direction must be known to an accuracy not worse than 10^{-4}. For this, very good calibration of the instrument is needed.

The speed and drift angle of the electrons depend on the electric field intensity, and this may have local inhomogeneities of static or dynamical origin.

Static inhomogeneities arise because of incorrect or inaccurate positioning of the field-shaping electrodes, the signal wires, and the screening grids, and also because of incorrect distribution of the voltage applied to the field-shaping electrodes. These shortcomings can be taken into account or eliminated by calibrating the drift chamber before the start of measurements.

Dynamical changes in w_d and α_M occur above all through the accumulation of space charge in the drift volume of the chamber, and also through changes in the temperature, pressure, and composition of the gas mixture. These changes can be taken into account only by means of continuous calibration of the chamber during an experiment.

Methods of calibration

For track reconstruction in multilayer drift chambers, three methods of calibration are used: by beam particles, autocalibration, and by a laser beam. The first method is suitable only for chambers in experiments with fixed-target accelerators with the beam passing through the chamber. Autocalibration is done by means of the tracks of the measured particles. If the connection between w_d and α_M in each layer of the multilayer chamber is known, then on the basis of a comparison of them one can estimate the local inhomogeneities of the electric field and introduce the necessary corrections in the track reconstruction.

The use of laser radiation to calibrate multilayer drift chambers is very popular (Refs. 15, 40, and 106–110). A laser beam imitates a straight track with an accuracy better than 20 μm.[110] This method is convenient for imitating straight tracks in detectors placed in a magnetic field. The main problem associated with the use of lasers with ultraviolet radiation is that their energy (a nitrogen laser, for example, emits photons with wavelength 337 nm and energy $h\nu = 3.7$ eV) is insufficient for ionization of not only argon ($I_0 = 15.76$ eV) but also the organic gases used in proportional detectors. The ionization of these mixtures by the laser radiation is explained by the presence of processes of double (Fig. 25a) or two-step (Fig. 25b) absorption of photons. Ionization of the gas by the laser radiation takes place with high probability through the second process, which presupposes the presence in the molecule of an intermediate

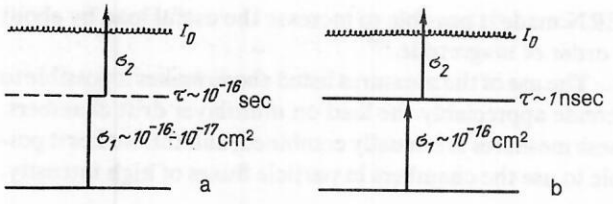

FIG. 25. Processes of double absorption (a) and two-step absorption (b) of photons.[15]

state with long lifetime ($\tau \geqslant 1$ nsec) and cross section $\sigma_1 \approx 10^{-16}$ cm². The theory of this phenomenon is set forth, for example, in Ref. 111.

Ionization by a laser is possible only if the gas contains admixtures of organic molecules with low ionization potential I_0, for example, nickelocene ($Ni(C_2H_5)_2$, $I_0 = 6.5$ eV), triethylamine (TEA, C_6H_{15}, $I_0 = 7.5$ eV), dimethylaniline (DMA, $C_8H_{11}N$, $I_0 = 7.14$ eV), diethylanine (DEA, $C_{10}H_{15}N$, $I_0 = 6.99$ eV), tetrakis (dimethylamino) ethylene (TMAE, $C_{10}H_{24}N_4$, $I_0 = 5.36$ eV).[112] These gases or vapors are added to the proportional detectors, and the density of ionization by the laser beam corresponds to the amount of gas with low ionization potential.[15,112]

It was shown in Refs. 15 and 107 that the ionization of the gas in a proportional detector (for example, Ar/CO_2, Ar/C_2H_6) also occurs effectively without the addition of a gas with a low ionization potential. This is explained by the fact that the concentration of such a gas can be extremely small (10^{-12}, Ref. 15). Such small admixtures are always present in the gas, since the purity of a mixture of commercial gases is usually $\sim 10^{-6}$–10^{-5}. For the calibration of large multilayer drift chambers, laser beams with an extension of more than 4 m are created (by means of a suitable optical focusing system). The laser pulse duration is usually about 300 nsec. To produce ionization corresponding to the specific ionization losses of a minimally ionizing particle (in argon, ≈ 100 electrons/cm), the laser beam must have an energy density $\geqslant 10\,\mu J/mm^2$ (Ref. 108).

Change in the characteristics of drift chambers during prolonged use

If proportional or drift chambers are used for a long time in strong particle beams, a decrease in their efficiency is observed. The same effect, called ageing, is also found in large multilayer drift chambers that operate under conditions of high radiation in colliding beams. For example, in the AFS chamber[69] a decrease of the gas multiplication by 15% was observed after two years of operation. During this time, $3 \cdot 10^{16}$ electrons were incident on each millimeter of wire. Ageing is also reflected in a displacement of the measured spectra of the ionization energy losses to lower amplitudes and a shortening of the plateau of the counting characteristic, and it may ultimately lead to snapping of a wire.

Wire "contamination" mechanism

The ageing effect is brought about by the deposition and polymerization of organic compounds on the surface of the electrodes in the chamber. As an example, Fig. 26 shows some signal wires after prolonged operation in proportional chambers filled with different gases.

The polymerization of hydrocarbons from the gas mixture is a multistage process. For example, in the mixture Ar + CH_4 the reactions

$$\left.\begin{aligned} &CH_4 + CH_2 \rightarrow C_2H_6, \\ &C_2H_6 + CH_2 \rightarrow C_3H_8, \text{ etc.,} \end{aligned}\right\} \qquad (30)$$

occur. This process continues until a compound is formed in the solid state (polymer), this attaching itself under the influence of the electric forces to the wire. The radicals (CH_2) that participate in the reactions of the type (30) are formed by the dissociation of organic molecules in the process of gas multiplication.

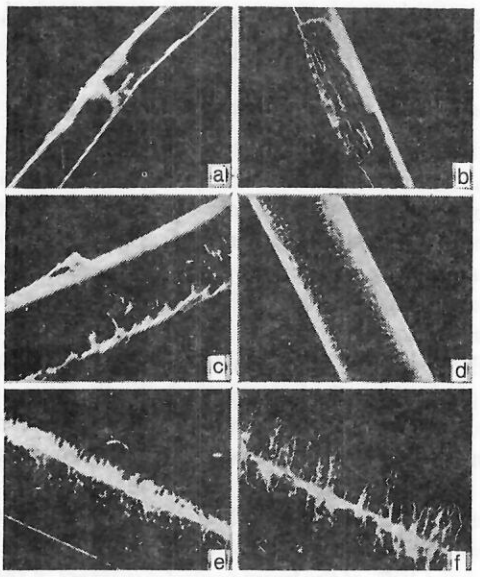

FIG. 26. Deposits on signal wires of drift chambers filled with: a) Ar + C_2H_6; b) Ar + C_2H_6 + methylal; c) Ar + CO_2; d), e), f) chambers of different constructional materials filled with Ar + CO_2.[113]

During the study of the ageing effect, an interesting fact was noted, namely, that the main element that formed a deposit on the surface of the signal wires was silicon, which occurs in the composition of the construction materials (for example, glass-reinforced epoxy).[47,113,114] This is explained by the fact that polymers are not robust; they decay with time, the carbon and hydrogen are liberated, and it is above all silicon that remains on the wires. It was established[113] that deposits on the wires also arise without hydrocarbons, for example, in an Ar–CO_2 mixture (Fig. 26c), i.e., many factors are involved in the ageing effect. It was shown in Ref. 113 that in a 50 %Ar + 50 %C_2H_6 mixture the ageing effect became noticeable at a total flux of 10^{16} electrons per 1 mm length of wire.

Methods of reducing ageing

The methods of reducing ageing reduce to the following:

1. The use of minimal gas multiplication. This is the most natural measure for extending the life of proportional and drift chambers.

2. The use of gas or vapor additives that are not subject to polymerization. An additive of this kind is, for example, methylal, a 1–3% use of which prolongs the life of the chamber by several times compared with the use of an argon + hydrocarbon binary mixture.

3. The use of a gas mixture without hydrocarbons. A chamber filled with Ar + CO_2 operates stably up to a total load of 10^{17} electrons/mm.[113]

4. Choice of a suitable construction material of the chamber. In a chamber that does not contain glass-reinforced epoxy, silicon is not found in the deposit on the wires, and the principal components of the deposits are sulfur and chlorine. In this case the admissible load reaches $2\cdot10^{16}$ electrons/mm.

5. The use of metallic electrodes instead of wires as cathodes. Such chambers have withstood the greatest load: $(1.5–2)\cdot10^{17}$ electrons/nm. The authors of Ref. 113 could not explain this effect.

6. Chamber conditioning. This is done by blowing pure argon through the chamber with a voltage applied to the wires. In the argon atmosphere, the hydrocarbon part of the deposits is "burnt" and the chamber operates more efficiently after the conditioning.

5. WIDE-GAP DRIFT CHAMBERS

Wide-gap drift chambers are planar drift chambers with a long drift length, usually 10–20 cm but sometimes up to a meter. They are also called economic drift chambers because their principal advantage is the small number of channels per unit of sensitive area.

In recent years, such chambers have been introduced into many high-energy experiments: in large muon detectors,[115] in electromagnetic and hadronic calorimeters,[116,117] and in neutrino detectors.[118] They form part of the giant detectors looking for nucleon decays.[119,120] They are also used in astrophysics investigations outside the atmosphere. A necessary condition for the use of wide-gap drift chambers to detect multitrack events is the use of a multiple TCD digital converter and a rapid parallel amplitude–digital converter, ADC, which were already discussed in Sec. 3. The electronic requirements of wide-gap and multilayer drift chambers are basically the same.

Spatial resolution in wide-gap drift chambers

The spatial resolution in such chambers is determined in the first place by the diffusion, $\sigma_{D'}$, and instrumental, σ_A, terms of Eq. (3). Therefore, on the basis of (3) and (12) the rms error in the measurement of the coordinate in such a chamber is

$$\sigma_x = \sqrt{\sigma_{D'}^2 x + \sigma_A^2}. \qquad (31)$$

As an example, Fig. 27 gives the dependence $\sigma_x(x)$ measured in Ref. 121. This means that in a wide-gap drift chamber one can, for example, in a mixture of argon ($\approx$80%) and isobutane ($\approx$20%) at saturated drift velocity (for this, it is necessary to create a field $E = 500–700$ V/cm), have a spatial resolution $\sigma_x \approx 0.2$ mm for $x = 1$ cm, $\sigma_x \approx 0.4$ mm for $x = 10$ cm, $\sigma_x \approx 0.9$ mm for $x = 50$ cm, and $\sigma_x \approx 1.3$ mm for $x = 100$ cm.

Wide-gap drift chambers with electrodes

Wide-gap drift chambers with electrodes are made in various forms. One sometimes uses the "classical" construction (see Fig. 2c) with field-shaping electrodes in the form of wires to which a linearly decreasing potential is applied.[122] Because of the large number of such wires in large chambers, it is necessary to employ massive frames, and as a result the chambers become cumbersome. Large frames are unsuitable above all in calorimeters, in which there is usually a premium on compactness.

One of the ways of achieving very compact chambers is to use chamber walls with a honeycomb filling. Such walls (a few centimeters thick) are the main carrying element of the chamber construction, and large frames are not necessary. Chambers of this kind measuring 4×2 m were constructed, for example, for the "Neĭtrinnyĭ detektor"" (neutrino detector) facility.[118] One of the modules of such a chamber is shown schematically in Fig. 28. Four chambers are placed simultaneously in a single volume, and this greatly simplifies the construction and increases the particle detection efficiency. The right–left ambiguity is eliminated by a displacement of the signal wires relative to the center of the module by $\pm$0.75 mm (the even ones in one direction, and the odd ones in the other).

A compact light construction of wide-gap drift chambers can be created by using metallic strips on a glass-reinforced epoxy wall of the chamber instead of wires to shape the field in the chamber.[115,119,123] The arrangement of such a chamber is shown in Fig. 29. Such chambers are used in large muon detectors,[115,124] in detectors looking for nucleon decays,[119,120] or in astrophysical experiments on board satellites. In such chambers, electron drift over a length greater than 50 cm can be realized without loss of efficiency.

Some authors have noted distortions of the field between the strips precisely when a grounded metallic plane is situated near the chamber wall.[120,125] This happens, for example, in calorimeters in which drift chambers alternate with large metallic slabs. The field distortions arise because some lines of force close on the external ground, passing through the glass-reinforced epoxy between the metallic strips. The positive ions drift along these lines and accumu-

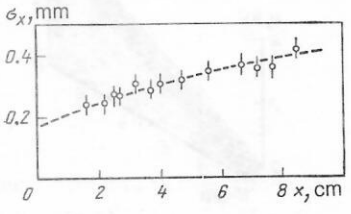

FIG. 27. Dependence of spatial resolution σ_x on the drift length in a wide-gap chamber filled with a mixture of 82% Ar and 18% iso-C_4H_{10}.[121] The curve corresponds to the dependence $\sigma_x = \sqrt{\sigma_{D'}^2 + \sigma_A^2}$ for $\sigma_{D'} = 124$ μm/cm and $\sigma = 170$ μm.

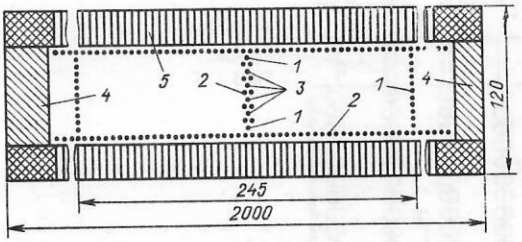

FIG. 28. Arrangement of a wide-gap drift chamber[118]: screening and cathode wires; 2) field-shaping wires; 3) signal wires; 4) sides; 5) honeycomb panels.

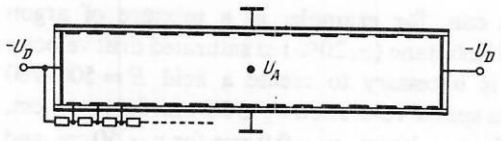

FIG. 29. Arrangement of a wide-gap drift chamber with field-shaping electrodes in the form of strips on glass-reinforced epoxy.

late on the surface of the insulator. As a result, the electric field in the chamber is deformed. Different methods have been proposed to eliminate this effect,[119,125] for example, the use of a high positive voltage on the anode and grounding of the cathode.[125]

It should be noted that wide-gap drift chambers with field-shaping electrodes in the form of strips work very reliably,[123,124] a striking example of which is the continuous operation for five years of 618 such chambers in the muon detector in the JADE facility in the e^+e^- collider PETRA at DESY.[115]

A very interesting example of the use of wide-gap drift chambers in high-energy physics is the precise measurement of the coordinates of high-energy electromagnetic showers initiated by γ rays and electrons. An example is the "high-density projection chamber"[116,126] used as an electromagnetic calorimeter in the DELPHI facility at CERN. The calorimeter has most impressive dimensions, 20 000 wires, and a mass of about 100 tons. The arrangement of the calorimeter is shown in Fig. 30. The electrons drift in channels of width 8 mm up to a distance of 65 cm. The lead walls of the channels are γ-ray converters, and are also used to shape the electric field. A linearly decreasing voltage is applied to sections of them made of an insulating material. The electrons are detected in proportional tubes placed directly at the end of the drift channels. Such a calorimeter measures the coordinates of electromagnetic showers with very high accuracy.

Wide-gap drift chambers are also used as additional coordinate detectors in a shower γ detector.[117,127] In front of it is a converter and immediately after it a wide-gap drift chamber. The signal from the latter is sent to a rapid parallel amplitude–digital converter, by means of which an "image" of the distribution of the charge released by the electromagnetic shower in the drift chamber is obtained. The position of the maximum of the charge distribution determines the coordinates of the shower axis.[127] This method was used to obtain a record spatial resolution for measurement of the coordinates of electromagnetic showers.[117,127]

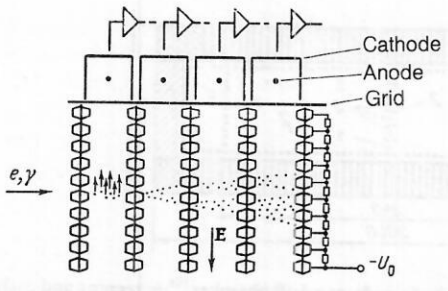

FIG. 30. Arrangement of an electromagnetic calorimeter based on a drift projection chamber.[116]

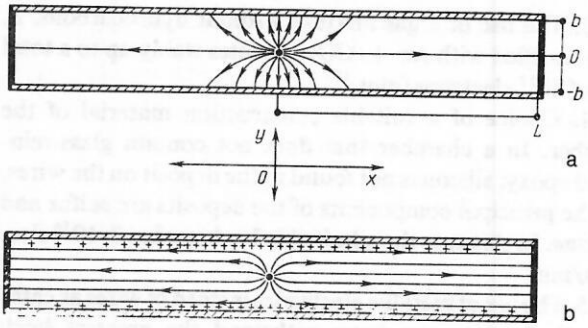

FIG. 31. Arrangement of an electrodeless drift chamber with the form of the lines of force: a) at the time of application of the voltage U_A; b) in the equilibrium state with accumulated charge on the insulator surface.

Electrodeless wide-gap drift chambers

An interesting new type of wide-gap drift chamber has recently been developed; it is the electrodeless drift chamber (Refs. 121, 125, and 128–131). The term "electrodeless" is used because the chamber does not have field-shaping electrodes and retains only the two basic electrodes—an anode in the form of a thin wire in the center of the chamber and a cathode placed at the far end of the chamber (Fig. 31). The walls of the chamber are made of an insulator (usually glass-reinforced epoxy); on their outer side they are metallized and grounded.

A positive voltage U_A is applied to the anode; the cathode is grounded. When the voltage is applied, the lines of force close through the insulator onto the exterior grounded screen (Fig. 31a). The positive ions that arise in the process of gas multiplication near the anode drift along the lines of force and attach themselves to the surface of the insulator. The accumulation of positive charge on the surface of the walls deforms the lines of force, and at the end of the self-

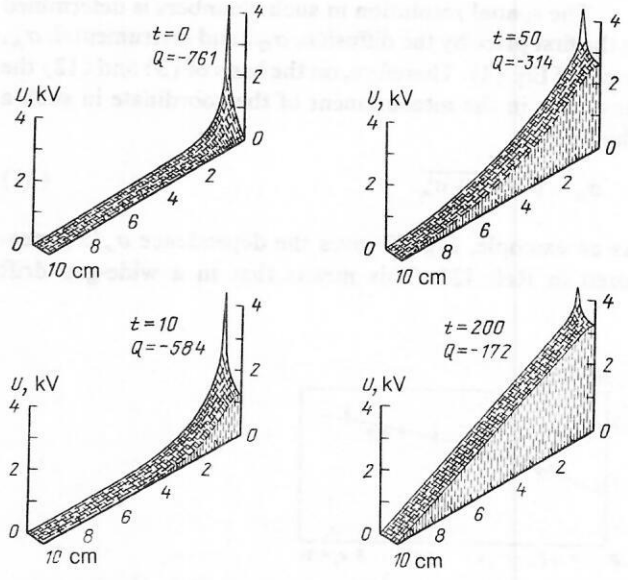

FIG. 32. Calculated electrostatic potential as a function of the distance x to the signal wire in an electrodeless drift chamber at different times t (rel. units) after application of a voltage $U_A = 4$ kV (Ref. 125); Q is the charge on the wire (rel. units).

regulating process of charge accumulation they are all directed toward the cathode at the far end of the chamber (Fig. 31b). Thus, an "ideal" electric field arises in the drift chamber.

The process of charging of the insulating surface was demonstrated in Ref. 125. Figure 32 shows the calculated time dependence of the distribution of the potential in an electrodeless chamber with walls of a perfect insulator. The electric field in the chamber at the time of charging of the anode ($t = 0$) is strongly inhomogeneous, with a large gradient near the wire. The electric field in the drift volume is increased and becomes homogeneous, its gradient near the wire decreasing. The ideal field for the drift chamber is achieved in the equilibrium state, shown in Fig. 32 ($t = 200$).

We obtain the potential in the "ideally" charged electrodeless drift chamber as a solution of the Laplace equation[132]:

$$\Phi(x,\ y) = U_A \left\{ \frac{L}{b} - \frac{1}{\pi} \ln \left[\sin^2 \left(\frac{\pi y}{2b} \right) + \sinh^2 \left(\frac{\pi x}{2b} \right) \right] \right\} \Big/ \left[\frac{L}{b} - \frac{2}{\pi} \ln \left(\frac{\pi a}{2b} \right) \right], \quad (32)$$

where the coordinate system and notation correspond to Fig. 31, and a is the radius of the wire. The expression (32) is valid for $b \ll L$. The potential near the wire is

$$\Phi(r) = U_A \left[\frac{L}{b} - \frac{2}{\pi} \ln \left(\frac{\pi r}{2b} \right) \right] \Big/ \left[\frac{L}{b} - \frac{2}{\pi} \ln \left(\frac{\pi a}{2b} \right) \right]. \quad (33)$$

The potential on the surface of the insulator at the point x is

$$\Phi(x,\ b) = U_A \left[\frac{L}{b} - \frac{2}{\pi} \ln \cosh \left(\frac{\pi x}{2b} \right) \right] \Big/ \left[\frac{L}{b} - \frac{2}{\pi} \ln \left(\frac{\pi a}{2b} \right) \right]. \quad (34)$$

The potential at the point $(0, b)$ is

$$\Phi(0,\ b) = U_A \Big/ \left[1 - \left(\frac{2b}{\pi L} \right) \ln \left(\frac{\pi a}{2b} \right) \right]. \quad (35)$$

The voltage difference ΔU between the signal wire and the wall of the chamber [the point $(0, b)$], which determines the gas multiplication, is

$$\Delta U = U_A \ln \left(\frac{\pi a}{2b} \right) \Big/ \left[\ln \left(\frac{\pi a}{2b} \right) - \frac{\pi L}{2b} \right]. \quad (36)$$

The charge density on the surface of the insulator at the point (x, b) is

$$q_s(x) = \Phi(x,\ b)\ \varepsilon/d, \quad (37)$$

where ε is the permittivity, and d is the thickness of the insulator.

Electrodeless chambers work stably and effectively (Refs. 121, 125, 128, 129, and 131–133). The intensity of cosmic rays on the surface of the earth is sufficient for complete charging of such a chamber. Various materials have been used as the walls of electrodeless chambers: glass-reinforced epoxy (Refs. 121, 125, 130, and 131), epoxide resin,[129] polyethylene,[128] polypropylene,[128,133] and plastic.[128] An attempt to use window glass[128] was unsuccessful. Electrodeless chambers of various configurations have been investigated: flat chambers with drift length up to 50 cm,[125,128] cylindrical chambers,[129,133] and also drift tubes, in which effective electron drift up to 1.2 m was achieved.[128,134] The principle of automatic regulation of the electric field in an electrodeless drift chamber makes it possible to create a homogeneous field in regions with a complicated configuration, and this may be very attractive for the use of such chambers in roentgenography, nuclear spectroscopy, etc.

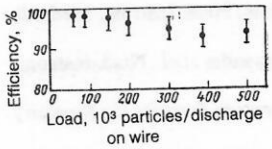

FIG. 33. Efficiency of an electrodeless chamber as a function of the particle flux.[121]

Originally, electrodeless drift chambers were used only in low-intensity beams or in cosmic rays. In Refs. 121 and 131 it was shown that they can also work effectively and reliably under conditions typical of accelerators.

In electrodeless chambers there exist specific effects such as a leakage current through the insulating wall of the chamber and along its surface, diffusion of ions, etc. The leakage current reduces the charge density on the surface of the insulator, and this leads to the formation of a focusing electric field in the chamber; ion diffusion leads, conversely, to an increase in the charge density and to the appearance of a defocusing field. These questions are considered, for example, in Refs. 121, 132, and 133.

In strong particle fluxes, these effects play an important part; the charge density on the surface of the insulator increases, ΔU [see (36)] decreases, and as a result the signal amplitude falls. However, it has been shown[121,131] that a new—dynamical—equilibrium is established in the chamber, which then works stably but with a lower gas multiplication coefficient M. A particular property of electrodeless chambers is the very weak dependence of M on the anode voltage. Therefore, it is virtually impossible in such chambers to regulate the amplitude by changing U_A. If more sensitive amplifiers are used, an electrodeless drift chamber can work with high efficiency in a particle flux of $5 \cdot 10^5$ sec^{-1} per wire (Fig. 33),[121,131] this corresponding under collider conditions to a uniform particle flux of $\sim 3 \cdot 10^6$ m$^{-2} \cdot$sec^{-1}. Such a load is the limit for a wide-gap drift chamber with a drift length of about 10 cm (electron collection time of about 2 μsec) if one is to be able to distinguish tracks of the measured event from the tracks of particles that pass through the chamber earlier or later.

Good spatial resolution can be achieved in an electrodeless drift chamber. For example, the dependence of the spatial resolution on the drift length shown in Fig. 27 was measured in an electrodeless drift chamber.[121] The spatial resolution and the drift-time–coordinate ratio are practically independent of the particle flux.[131]

Electrodeless drift chambers are distinguished by their simple construction and low cost. They can be successfully used in large muon detectors, in electromagnetic and hadronic calorimeters, in experiments looking for nucleon decay, and in cosmic-ray detectors.

I should like to thank Yu. A. Budagov and G. I. Merzon for discussing my draft and for valuable comments, and L. Sitarova for assistance in preparing the text.

[1]T. Bresani, G. Charpak, D. Rahm *et al.*, in: *Proc. of the Seminar on Filmless and Streamer Chambers*, Dubna (1969), p. 275.
[2]G. Charpak, D. Rahm, and H. Steiner, Nucl. Instrum. Methods **80**, 13 (1970).

[3]A. H. Walenta, J. Heintze, and B. Schurlein, Nucl. Instrum. Methods **92**, 373 (1971).
[4]J. Saudinos, J.-C. Duchazeaubeneix, C. Laspalles *et al.*, Nucl. Instrum. Methods **111**, 77 (1973).
[5]Yu. V. Zanevskiĭ, *Wire Detectors of Elementary Particles* [in Russian] (Atomizdat, Moscow, 1978).
[6]P. Rice-Evans, *Spark, Streamer, Proportional and Drift Chambers* (Richelieu Press, London, 1974).
[7]F. Sauli, "Principles of operation of multiwire proportional and drift chambers," Preprint CERN 77-09, Geneva (1977).
[8]G. Charpak and F. Sauli, Ann. Rev. Nucl. Part. Sci. **34**, 285 (1984).
[9]G. I. Merzon, B. Sitar, and Yu. A. Budagov, Fiz. Elem. Chastits At. Yadra **14**, 648 (1983) [Sov. J. Part. Nucl. **14**, 270 (1983)].
[10]G. D. Alekseev, V. I. Ganichev, O. E. Gorchakov *et al.*, Prib. Tekh. Eksp. No. 2, **52** (1985).
[11]G. D. Alekseev, V. V. Kruglov, and D. M. Khazine, Fiz. Elem. Chastits At. Yadra **13**, 703 (1982) [Sov. J. Part. Nucl. **13**, 293 (1982)].
[12]A. Peisert and F. Sauli, Preprint CERN 84-08, Geneva (1984).
[13]G. Schultz and J. Gresser, Nucl. Instrum. Methods **151**, 413 (1978).
[14]J. A. Jaros, "Drift and proportional tracking chambers," SLAC-PUB-2647, SLAC (1980).
[15]B. Sadoulet, in: *Proc. of the Inter. Conf. on Instrumentation for Colliding Beam Physics*, SLAC (1982), p. 1.
[16]F. Lapique and F. Piuz, Nucl. Instrum. Methods **175**, 297 (1980).
[17]A. H. von Engel, *Ionized Gases* (Clarendon Press, Oxford, 1955) [Russ. transl., Fizmatgiz, Moscow, 1959].
[18]S. C. Brown,*Basic Data of Plasma Physics* (MIT Press, Cambridge, Mass., 1959) [Russ. transl., Gosatomizdat, Moscow, 1961].
[19]J. B. Hasted, *Physics of Atomic Collisions* (Butterworths, London, 1964) [Russ. transl., Mir, Moscow, 1965].
[20]L. G. H. Huxley and R. W. Crompton, *The Diffusion and Drift of Electrons in Gases* (Wiley–Interscience, New York, 1974) [Russ. transl., Mir, Moscow, 1977].
[21]E. W. McDaniel, *Collision Phenomena in Ionized Gases* (Wiley, New York, 1964) [Russ. transl., Mir, Moscow, 1967].
[22]L. S. Frost and A. V. Phelps, Phys. Rev. **127**, 1621 (1962).
[23]B. M. Smirnov, *Atomic Collisions and Elementary Processes in Plasmas* [in Russian] (Atomizdat, Moscow, 1968).
[24]V. Palladino and B. Sadoulet, Nucl. Instrum. Methods **128**, 323 (1975).
[25]E. B. Wagner, F. J. Davis, and G. S. Hurst, J. Chem. Phys. **47**, 3138 (1967).
[26]J. H. Parker and J. J. Lowke, Phys. Rev. **181**, 290 (1969).
[27]H. R. Skullerud, J. Phys. B **2**, 696 (1969).
[28]F. Puiz, Nucl. Instrum. Methods **205**, 425 (1983).
[29]N. A. Filatova, T. S. Nigmanov, V. P. Pugachevich *et al.*, Nucl. Instrum. Methods **143**, 17 (1977).
[30]H. Drumm, R. Eichler, B. Granz *et al.*, Nucl. Instrum. Methods **176**, 333 (1980).
[31]P. Villa, Nucl. Instrum. Methods **217**, 273 (1983).
[32]S. Bobkov, V. Cherniatin, B. Dolgoshein *et al.*, Nucl. Instrum. Methods **226**, 376 (1984).
[33]A. H. Walenta, J. Fehlmann, H. Hofer *et al.*, in *Proc. of the Intern. Conf. on Instrumentation for Colliding Beam Physics*, SLAC (1982), p. 34.
[34]R. A. Boie, A. T. Hrisoho, and P. Rehak, IEEE Trans. Nucl. Sci. **NS-28**, 603 (1981).
[35]Yu. A. Budagov V. Glinka A. P. Nagaĭtsev *et al.*, Preprint 13-84-337 [in Russian], JINR, Dubna (1984).
[36]P. Duinker, J. C. Guo, D. Harting *et al.*, Nucl. Instrum. Methods **201**, 351 (1982).
[37]J. Va'vra, Nucl. Instrum. Methods **217**, 322 (1983).
[38]V. Commichau, K. H. Dederichs, M. Deutschmann *et al.*, Nucl. Instrum. Methods **A239**, 487 (1985).
[39]A. A. Carter, J. R. Carter, G. Ero *et al.*, Nucl. Instrum. Methods **225**, 308 (1984).
[40]D. Bettoni, B. Dolgoshein, C. W. Fabjan *et al.*, Nucl. Instrum. Methods **A236**, 264 (1985).
[41]J. Va'vra, Nucl. Instrum. Methods **A244**, 391 (1986).
[42]E. D. Platner, in: *Proc. of the Intern. Conf. on Instrumentation for Colliding Beam Physics*, SLAC (1982), p. 24.
[43]S. Eiseman, A. Etkin, K. J. Foley *et al.*, IEEE Trans. Nucl. Sci. **NS-50**, 149 (1983).
[44]Yu. I. Davydov, S. V. Sergeev, P. Strmen' *et al.*, Preprint 13-86-730 [in Russian], JINR, Dubna (1986).
[45]G. Charpak, S. Majewski, and F. Sauli, Nucl. Instrum. Methods **126**, 381 (1975).
[46]V. I. Baskakov, V. K. Chernjatin, B. A. Dolgoshein *et al.*, Nucl. Instrum. Methods **158**, 129 (1979).
[47]H. Sipilä and M. L. Järvinen, Nucl. Instrum. Methods **217**, 298 (1983).
[48]A. D. Volkov, V. M. Grebenyuk, B. Zh. Zalikhanov *et al.*, Preprint 13-85-418 [in Russian], JINR, Dubna (1985).
[49]W. W. M. Allison and F. R. S. Wright, in *Formulae and Methods in Experimental Data Evaluation*, Vol. 2, edited by R. K. Bock (European Phys. Soc., Geneva, 1984), p. E1.
[50]W. W. M. Allison, C. B. Brooks, J. N. Bunch *et al.*, Nucl. Instrum. Methods **119**, 499 (1974).
[51]A. R. Clark, O. Dahl, P. Eberhard *et al.*, "Proposal for PEP facility based on time projection chamber," PEP Exp. No. 4 (1976).
[52]W. W. M. Allison, Phys. Scr. **23**, 348 (1981)
[53]G. R. Lynch and N. J. Hadley, in: *Proc. of the Intern. Conf. on Instrumentation for Colliding Beam Physics*, SLAC (1982), p. 85.
[54]A. Wagner, in: *Proc. of the Intern. Conf. on Instrumentation for Colliding Beam Physics*, SLAC (1982), p. 76.
[55]M. Calvetti, P. Cennini, S. Centro *et al.*,in: *Proc. of the Intern. Conf. on Instrumentation for Colliding Beam Physics*, SLAC (1982), p. 16.
[56]W. W. M. Allison, C. B. Brooks, and P. D. Shield, Nucl. Instrum. Methods **224**, 396 (1984).
[57]D. Goloskie, V. Kistiakowski, S. Oh *et al.*, Nucl. Instrum. Methods **A238**, 61 (1985).
[58]A. I. Babaev, D. A. Barskiĭ, S. D. Boris *et al.*, Preprint ITÉF-103 [in Russian], Moscow (1978).
[59]H. M. Braun, in: *Proc. of the Workshop on SPS Fixed-Target Physics*, CERN 83-02 (1983), p. 97.
[60]Yu. A. Budagov, V. B. Vinogradov, V. Glinka *et al.*, Preprint UKJF 80-83 [in Russian], Bratislava (1980).
[61]S. Benso, G. Darbo, I. Rossi *et al.*, Nucl. Instrum. Methods **217**, 194 (1983).
[62]D. A. Budilov, Yu. V. Zanevskiĭ, and Yu. Zlomanchuk, Prib. Tekh. Eksp. No. 2, 48 (1985).
[63]A. Wagner, Phys. Scr. **23**, 446 (1981).
[64]H. Aihara, J. M. Alston, D. H. Badtke *et al.*, IEEE Trans. Nucl. Sci. **NS-30**, 63 (1983).
[65]P. Delpierre, Nucl. Instrum. Methods **225**, 566 (1984).
[66]W. Blum, Nucl. Instrum. Methods **225**, 557 (1984).
[67]T. Kamae, H. Aihara, and R. Enomoto, Nucl. Instrum. Methods **252**, 423 (1986).
[68]H. Heintze, Nucl. Instrum. Methods **196**, 293 (1982).
[69]D. Cockerill, C. W. Fabjan, P. Frandsen *et al.*, Phys. Scr. **23**, 649 (1981).
[70]H. Roehrig, K. Einsweilar, D. Hutchison *et al.*, Nucl. Instrum. Methods **226**, 319 (1984).
[71]OPAL Collaboration, Technical Proposal CERN/LAPC/83-4 (1983).
[72]D. Theriot, Preprint FNAL-Conf. 84/71 (1984).
[73]W. B. Atwood, J. Carr, G. Chadwick *et al.*, Nucl. Instrum. Methods **A252**, 295 (1986).
[74]"Technical proposal for the H1 detector," DESY (1986).
[75]V. M. Auluchenko, B. I. Khazin, E. P. Solodov, and I. C. Snopkov, Nucl. Instrum. Methods **A252**, 299 (1986).
[76]G. G. Hanson, Nucl. Instrum. Methods **A252**, 343 (1986).
[77]M. Hasemann, in: *Proc. of the Intern. Conf. on Instrumentation for Colliding Beam Physics*, SLAC (1982), p. 80.
[78]M. Boerner, H. M. Fisher, H. Hartmann *et al.*, Nucl. Instrum. Methods **176**, 151 (1980).
[79]U. Binder, W. de Boer, G. Grindhammer *et al.*, Nucl. Instrum. Methods **217**, 285 (1983).
[80]W. T. Ford, in: *Proc. of the Intern. Conf. on Instrumentation for Colliding Beam Physics*, SLAC (1982).
[81]D. G. Cassel, R. Desalvo, J. Dobbins *et al.*, Nucl. Instrum. Methods **A252**, 325 (1986).
[82]K. Eggert, C. Engster, L. Van Koningsveld *et al.*, Nucl. Instrum. Methods **176**, 223 (1980).
[83]D. Ouimette, IEEE Trans. Nucl. Sci. **NS-29**, 290 (1982).
[84]C. Lagrele and J. C. Lugol, IEEE Trans. Nucl. Sci. **NS-30**, 297 (1983).
[85]Yu. A. Budagov, M. Seman, A. A. Semenov *et al.*, Nucl. Instrum. Methods **A234**, 302 (1985).
[86]B. Hallgren and H. Werveij, IEEE Trans. Nucl. Sci. **NS-27**, 333 (1980).
[87]Yu. A. Budagov, V. G. Zinov, M. Seman *et al.*, Preprint 13-85-585 [in Russian], JINR, Dubna (1985).
[88]A. M. Batrakov and V. P. Kozak, Preprint No. 85-10 [in Russian] Institute of Nuclear Physics, Novosibirsk (1985).
[89]V. Radeka, IEEE Trans. Nucl. Sci. **NS-21**, 51 (1974).
[90]G. A. Erskine, Nucl. Instrum. Methods **105**, 565 (1972); **198**, 325 (1982).
[91]D. Nygren, Phys. Scr. **23**, 584 (1981).
[92]L. S. Barabash, A. M. Baranov, G. B. Bondarenko *et al.*, Nucl. Instrum. Methods **A236**, 271 (1985).
[93]R. Janik, L. Moucka, V. D. Pesechonov, and B. Sitar, Nucl. Instrum. Methods **178**, 71 (1980).

[94]S. H. Aronson, Preprint BNL-34525 OG 772, Brookhaven (1984).
[95]A. R. Erwin, H. Chen, A. Hasan *et al.*, Nucl. Instrum. Methods **A237**, 439 (1985).
[96]D. F. Anderson, H. K. Arvela, A. Breskin, and G. Charpak, Preprint CERN EP/84-01 (1984).
[97]J. Allison, R. J. Barlow, R. Canas *et al.*, Nucl. Instrum. Methods **A236**, 284 (1985).
[98]T. Miki, R. Itoh, and T. Kamae, Nucl. Instrum. Methods **A236**, 64 (1985).
[99]F. Sauli, in: *The Time Projection Chamber*, edited by J. A. MacDonald (AIP, New York, 1984), p. 171.
[100]U. Becker, M. Capell, M. Chen *et al.*, Nucl. Instrum. Methods **214**, 525 (1983).
[101]P. Nemethy, P. J. Oddone, N. Toge, and A. Ishibashi, Nucl. Instrum. Methods **212**, 273 (1983).
[102]I. Lehraus, R. Matthewson, and W. Tejessy, Nucl. Instrum. Methods **196**, 361 (1982).
[103]D. A. Bryman, M. Leitch, I. Navon *et al.*, Nucl. Instrum. Methods **A234**, 42 (1985).
[104]S. R. Amendolia, W. Blum, R. Benetta *et al.*, Nucl. Instrum. Methods **A234**, 47 (1985).
[105]M. Dameri, G. Darbo, E. Lamanna *et al.*, Nucl. Instrum. Methods **A235**, 279 (1985).
[106]B. Sadoulet, Phys. Scr. **23**, 434 (1981).
[107]H. J. Hilke, Nucl. Instrum. Methods **174**, 145 (1980).
[108]I. Lehraus, Nucl. Instrum. Methods **217**, 43 (1983).
[109]J. Va'vra, Nucl. Instrum. Methods **225**, 13 (1984).
[110]S. R. Amendolia, W. Blum, R. Benetta *et al.*, Nucl. Instrum. Methods **A235**, 296 (1985).
[111]E. M. Gushchin, A. N. Lebedev, and S. V. Somov, Nucl. Instrum. Methods **228**, 94 (1984).
[112]K. W. D. Ledingham, C. Raine, K. M. Smith *et al.*, Nucl. Instrum. Methods **225**, 319 (1984).
[113]J. Adam, Nucl. Instrum. Methods **217**, 291 (1983).
[114]M. Turala and J. C. Vermuelen, Nucl. Instrum. Methods **205**, 141 (1983).
[115]J. Allison, J. C. Armitage, J. T. Baines *et al.*, Nucl. Instrum. Methods **A238**, 220 (1985).
[116]A. Cattai, H. G. Fischer, P. S. Iversen *et al.*, Nucl. Instrum. Methods **A235**, 310 (1985).
[117]Yu. A. Budagov, A. A. Omelyanenko, A. A. Semenov *et al.*, Nucl. Instrum. Methods **A238**, 74 (1985).
[118]L. S. Barabash, I. A. Golutvin, Yu. A. Zlobin *et al.*, in: *Proc. of the Fifth Working Symposium on the Neutrino Detector*, IHEP–JINR, D1,2,13-84-332 [in Russian], Dubna (1984), p. 108.
[119]L. E. Price, J. Dawson, D. Ayres *et al.*, IEEE Trans. Nucl. Sci. **NS-29**, 383 (1982).
[120]L. E. Price, in: *Proc. of the Intern. Conf. on Instrumentation for Colliding Beam Physics*, SLAC (1982), p. 206.
[121]Yu. A. Budagov, V. V. Glagolev, V. M. Korolev *et al.*, Preprint 13-86-565 [in Russian], JINR, Dubna (1986).
[122]M. Rahman, I. Meyer, W. D. Dau *et al.*, Nucl. Instrum. Methods **188**, 159 (1981).
[123]Yu. A. Budagov, A. P. Nagaĭtsev, A. A. Omel'yanenko *et al.*, Preprint R1-84-546 [in Russian], JINR, Dubna (1984).
[124]K. A. Connel, R. A. Cunningham, M. Edwards *et al.*, Nucl. Instrum. Methods **144**, 453 (1977).
[125]J Allison, R. J. Barlow, C. K. Bowdery *et al.*, Nucl. Instrum. Methods **201**, 341 (1982).
[126]M. Berggren, A. Cattai, H. G. Fischer *et al.*, Nucl. Instrum. Methods **225**, 477 (1984).
[127]G. S. Bitsadze, Yu. A. Budagov, and V. V. Glagolev, Nucl. Instrum. Methods **A251**, 61 (1986).
[128]Ch. Becker, W. Weihs, and G. Zech, Nucl. Instrum. Methods **200**, 335 (1982).
[129]A. Franz and C. Grupen, Nucl. Instrum. Methods **200**, 331 (1982).
[130]D. S. Ayres and L. E. Price, Preprint ANL-HEB-CP-82-34 (1982).
[131]Yu. A. Budagov, A. P. Nagajcev, A. A. Omelyanenko *et al.*, Nucl. Instrum. Methods **A238**, 245 (1985).
[132]Ch. Becker, W. Weihs, and G. Zech, Nucl. Instrum. Methods **213**, 243 (1983).
[133]R. Dorr, C. Grupen, and A. Noll, Nucl. Instrum. Methods **A238**, 245 (1985).
[134]G. Zech, Nucl. Instrum. Methods **217**, 209 (1983).

Translated by Julian B. Barbour